

Geochemistry, Geophysics, Geosystems[®]



RESEARCH ARTICLE

10.1029/2021GC009795

Key Points:

- We examine clinkers, which are pyro-metamorphic rocks formed by coal seam fires, as a new candidate material for paleointensity studies
- We find clinker products contain three main magnetic minerals: magnetite, hematite, and the rare ϵ - Fe_2O_3
- Overall, our rock magnetic results suggests that clinkers should be reliable paleomagnetic full vector recorders

Supporting Information:

Supporting Information may be found in the online version of this article.

Correspondence to:

C. J. Sprain,
C.Sprain@liverpool.ac.uk

Citation:

Sprain, C. J., Feinberg, J. M., Lamers, R., & Bono, R. K. (2021). Characterization of magnetic mineral assemblages in clinkers: Potential tools for full vector paleomagnetic studies. *Geochemistry, Geophysics, Geosystems*, 22, e2021GC009795. <https://doi.org/10.1029/2021GC009795>

Received 17 MAR 2021

Accepted 31 AUG 2021

Characterization of Magnetic Mineral Assemblages in Clinkers: Potential Tools for Full Vector Paleomagnetic Studies

Courtney J. Sprain^{1,2} , Joshua M. Feinberg³ , Riley Lamers³, and Richard K. Bono¹ 

¹Department of Earth, Ocean and Ecological Sciences, University of Liverpool, Liverpool, UK, ²Now at Department of Geological Sciences, University of Florida, Gainesville, FL, USA, ³Department of Earth and Environmental Science, University of Minnesota, Minneapolis, MN, USA

Abstract High-quality paleointensity data are essential for improving our understanding of the geomagnetic field; however, it is challenging to find materials that reliably record full vector magnetization going back in time. Here, we examine a new candidate material for paleointensity studies: clinkers, which are rocks that have been baked, metamorphosed, or melted by underlying coal seam fires. Previous studies conducted on clinkers suggest that they may be high-fidelity magnetic field recorders. However, due to the inhomogeneity of clinker deposits and limited scope of previous studies, it is unknown under what conditions these conclusions hold true. To better assess this, we quantified the variation of magnetic properties within clinker deposits collected from the Powder River Basin, Montana, as a function of lithology, oxidation state, distance from the coal seam, and location. Our results indicate that the clinker products contain three main magnetic minerals: magnetite, hematite, and the rare ϵ - Fe_2O_3 . Clinker lithology was found to be the primary control on magnetic mineralogy, where strongly baked sediment and porcellanite are dominated by varying proportions of hematite, ϵ - Fe_2O_3 , and magnetite, and paralavas are dominated by low-Ti magnetite. All clinker materials are thermally stable and likely experienced temperatures in excess of the magnetite Curie temperature. Grain size analysis indicates that the magnetic particles in all clinker materials are amenable to high-quality paleointensity study. In total, our study confirms that clinkers should be reliable full vector paleomagnetic recorders.

Plain Language Summary Measuring Earth's ancient magnetic field strength is challenging due to a paucity of reliable recorders. However, to understand how the geomagnetic field has behaved over time, robust records of field strength are necessary. Here, we examine clinkers, which are rocks that have been baked, metamorphosed, or welded by coal seam fires, as a potential new material for characterizing the ancient magnetic field strength. Prior study suggested that clinkers may be robust magnetic recorders. However, due to heterogeneity in clinker deposits, more extensive study is required to understand the extent of their suitability for paleomagnetic analysis. In our study, we quantified the variation of magnetic properties within clinker deposits collected from the Powder River Basin, Montana, as a function of clinker rock type, oxidation state, distance from the coal seam, and location. Our results show that clinkers contain three main magnetic minerals: magnetite, hematite, and the rare ϵ - Fe_2O_3 ; the latter of which has so far only been found as a primary magnetic mineral in baked archeological artifacts. We found that clinker rock type is the primary control on magnetic mineralogy. Overall, the rock magnetic characteristics of clinkers suggest they should be reliable recorders of ancient magnetic field strength.

1. Introduction

High-quality paleomagnetic data are essential for documenting the variation in Earth's magnetic field on geologic timescales. These variations provide insight into the magnetohydrodynamic processes that occur in Earth's outer core, and additionally have important implications for a range of Earth processes including the deflection of the solar wind (Tarduno et al., 2010), cosmogenic nuclide production rates (Lifton et al., 2014), the evolution of the deep interior (Biggin et al., 2015), and habitability (Lammer et al., 2009). Currently, there are several global time-varying paleomagnetic field models for the Holocene, derived from paleomagnetic and archeomagnetic data that have greatly improved our understanding of the magnetic field for the last 10 kyr (e.g., Constable et al., 2016; Korte & Constable, 2003, 2011, 2005; Korte et al., 2011;

© 2021. The Authors.

This is an open access article under the terms of the [Creative Commons Attribution License](https://creativecommons.org/licenses/by/4.0/), which permits use, distribution and reproduction in any medium, provided the original work is properly cited.

Nilsson et al., 2014; Panovska et al., 2018; Pavón-Carrasco et al., 2014). Recently, Panovska et al. (2018) were able to push this understanding back to 100 ka with the release of GGF100k, a global time-varying field model for the past 100 kyr. This new model provided a huge step forward in understanding long-term variations in Earth's magnetic field, and in particular was able to resolve magnetic excursions. Despite the advancements represented in GGF100k, there still remain many opportunities to improve and expand upon this model.

In particular, GGF100k is severely lacking in absolute records of paleointensity. Absolute paleointensity data are important for providing records of field behavior in regions that lack long-duration sediment records and additionally are used to calibrate relative paleointensity records from sediment cores. Furthermore, absolute paleointensity data are intrinsically different than relative paleointensity data and they provide important "instantaneous" snapshots of the magnetic field that are not obtainable from sedimentary records. Of the approximately 85,000 paleomagnetic records that went into GGF100k, only ~15,000 were from volcanic rocks or archeological materials capable of recording absolute paleointensity. The distribution of these data in time was biased toward recent periods, with ~90% of the absolute paleointensity data falling within the last 10 kyr (encompassing all archeological data) due largely to a decrease in reliable recorders further back in Earth history. Additionally, large spatial gaps occur beyond 10 ka where volcanic samples amenable to paleointensity study are rare, such as within ancient sedimentary basins in continental interiors. Addressing these spatial and temporal gaps in absolute paleointensity data would help improve our understanding of long-term variations in Earth's magnetic field over the past 100 kyr. Ideally, global magnetic field models would be extended further back in time to characterize magnetic processes that occur on longer timescales, including magnetic reversals. However, there is not currently enough magnetic data to do this, and new high-quality full vector records of recent field behavior are needed.

A potential candidate for obtaining robust full vector paleomagnetic data are clinker deposits, a suite of pyro-metamorphic rocks that have been baked, welded, and/or melted by the natural burning of underlying coal beds (Coates & Heffern, 1999; Grapes, 2010). Clinkers are frequently found in continental interiors and have a wide geographic distribution, identified in at least 15 countries (Figure 1). Clinkers are attractive candidates for this work because they can be precisely dated using (U-Th)/He, $^{40}\text{Ar}/^{39}\text{Ar}$, and fission track geochronologic techniques (Estrada et al., 2009; Heffern et al., 2007; Novikov et al., 2008; Novikova et al., 2016; Reiners et al., 2011; Riihimaki & Reiners, 2012; Riihimaki et al., 2009; Sokol & Volkova, 2007; Sokol et al., 2014). Previous paleomagnetic and rock magnetic studies of clinker deposits suggest that they may be high-fidelity magnetic field recorders, possessing unambiguously clear and stable thermoremanent (TRM) or thermo-chemical remanent magnetizations (TCRMs) (Bucha et al., 1968; Cisowski & Fuller, 1987; de Boer et al., 2001; Hooper, 1987; Jones et al., 1984; Khesin et al., 2005; Krs, 1968; Krsová et al., 1989; Lindqvist et al., 1985; Rådan & Rådan, 1998; Ron & Kolodny, 1992; Sternberg, 2009; Sternberg et al., 2008). Although prior work shows the potential utility of some clinker materials for full vector studies, clinker deposits are inhomogeneous and a single deposit can display variable oxidation states, different primary lithologies, and contrasting degrees of thermal alteration. Thus, it is important to characterize the diversity of rock magnetic properties in clinker deposits, so that future workers can focus their research efforts on the portions of clinkers that are reliable recorders of Earth's magnetic field.

In this study, we characterize the magnetic mineral assemblage in clinker deposits collected from Custer National Forest in the Powder River Basin (PRB), SE Montana and their acquisition of magnetic remanence. Particular emphasis is placed on assessing how magnetic mineralogy varies with distance from the coal seam, lithology, oxidation state, and regionally, with a goal of identifying which part of a clinker, if any, has the requisite magnetic properties to be a high-fidelity recorder of the full vector paleomagnetic field.

2. Anatomy of Clinker Deposits and Geologic Setting

Naturally occurring coal bed fires are common in areas where coal beds are exposed near the surface above the water table. In the United States, coal fires are found in geologic basins within Wyoming, Montana, North Dakota, Colorado, Utah, Kentucky, West Virginia, Pennsylvania, and Alaska (Figure 1; Kuenzer & Stracher, 2012). Coal bed fires in these areas were also common in the past, as evidenced by extensive clinker outcrops, which in the PRB alone cover 4,100 km² (Heffern & Coates, 2004). Common mechanisms for

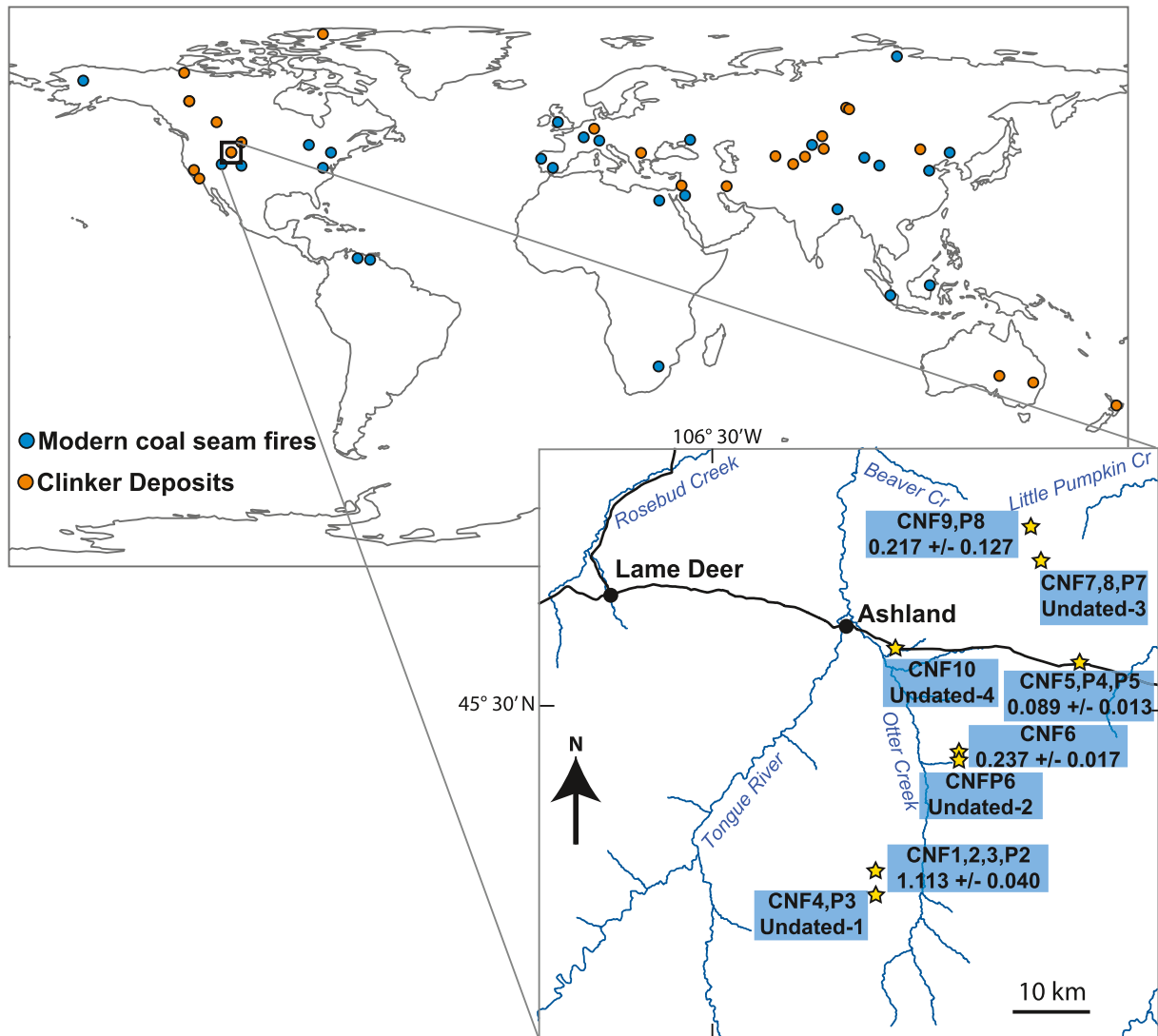


Figure 1. Location map of clinker deposits (orange) and coal seam fires (blue) around the world. Inset shows a map of sampling locations in Custer National Forest. Stars mark locations of sampled clinker deposits. Ages are in Ma with uncertainties stated at 2σ and are from Heffern et al. (2007), Reiners et al. (2011), Riihimaki et al. (2009), and Riihimaki and Reiners (2012). Coal locations taken from Stracher et al. (2010) and clinker locations summarized in Sokol and Volkova (2007).

coal fire ignition, not including human activity, are lightning, wildfires, and spontaneous combustion (Heffern & Coates, 2004). These fires are thought to start naturally at coal exposures near the surface and then retreat into the subsurface as the coal is combusted. In response, the overlying strata slump, fracture, and fault as the under burden is removed (Figure 2). Fractures act as conduits for bilateral air flow, bringing oxygen to the fire and allowing methane, carbon dioxide, and water vapor to escape. These fractures are generally subjected to the highest temperatures within the clinker, ranging from 1000°C to 2000°C (Grapes, 2010; Heffern & Coates, 2004; Kuenzer & Stracher, 2012). As coal seam fires recede further into the subsurface, they are eventually extinguished as their oxygen supply is exhausted, or as the fires intercept the water table. The thickness of the resulting clinker deposit is dependent upon the original thickness of the combusted coal bed (Grapes, 2010). Combustion can start again at a later point when after erosion, the remaining coal is once again exposed to the surface (Heffern et al., 2007). Of particular importance to paleomagnetic studies, due to the uneven nature of combustion, a single coal seam can result in multiple generations of clinker formation where the age of the clinker is not uniform across a horizon (Heffern et al., 2007).

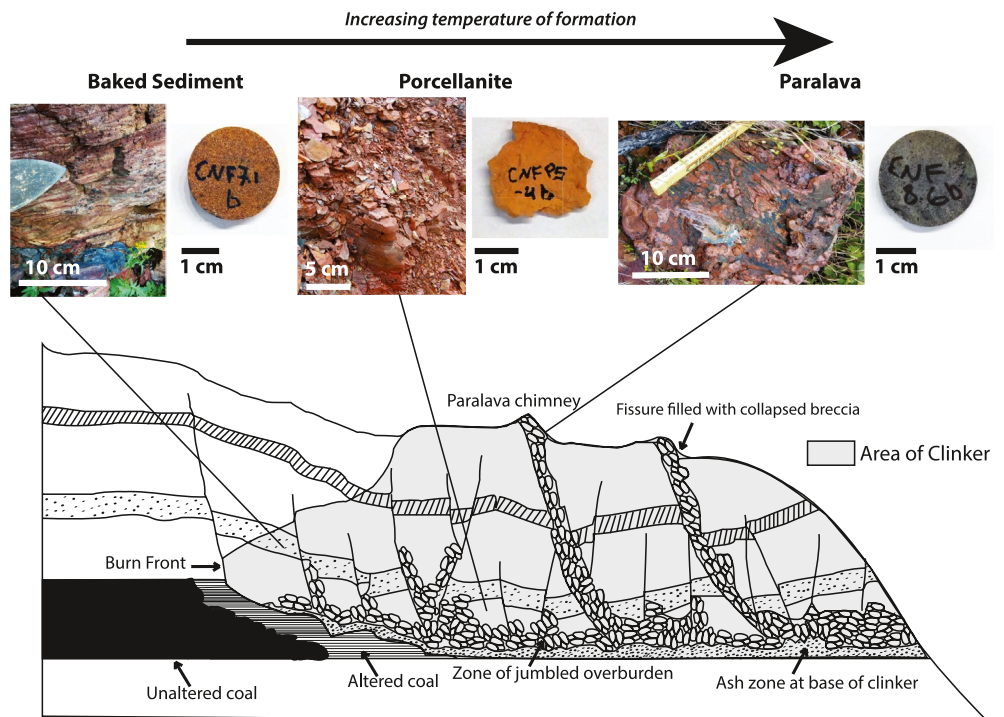


Figure 2. Schematic of cross section of coal seam fire propagating into a hillside. Photos show field examples and laboratory specimens of different clinker lithology types including strongly baked sediment, porcellanite, and paralava. Modified from Heffern and Coates (1997).

The term clinker applies to all metamorphic products formed by heating and chemical alteration during combustion of coal beds (Coates & Heffern, 2000; Sarnecki, 1991). The lithology of these units can be highly variable and is dependent upon the heat intensity, duration of exposure to heat, oxidation state, and initial composition (Coates & Heffern, 2000). The resulting products are classified into three categories: baked rocks, porcellanite-like rocks, and molten rocks or paralavas (Kuenzer & Stracher, 2012). In general, baked rocks form within more distal sediments to the coal seam fire, where temperatures are lower (300°C–800°C) and heat is transferred upwards from the coal seam via convection (Kuenzer & Stracher, 2012). Baked rocks experience dehydration and oxidation, resulting in pigmentation by hematite or limonite (Coates & Heffern, 2000). These baked sediments occasionally retain original sedimentary structures and tend to be well indurated. In general, the more intense alteration is closest to the burning coal. Porcellanite is recrystallized shale or siltstone with a ceramic texture that forms after exposure to temperatures between ~600°C and 1400°C (Coates & Heffern, 2000; Kuenzer & Stracher, 2012), and may occur in a reduced or oxidized state (Coates & Heffern, 2000). Paralava is melted rock, named for its vesicular texture and dark color, that forms when materials are heated to 1500–2000°C (Kuenzer & Stracher, 2012). Paralavas often occur next to vents or chimneys where escaped gases from incomplete combustion ignite as they are convected to the surface (Coates & Heffern, 2000). These environments are commonly reducing (Coates & Heffern, 2000). Welded breccias are also common in fractures and chimneys and are closely associated with paralavas (Heffern et al., 2007; Figure 2). Near the base of clinker deposits, collapsed overburden can create a brecciated layer of baked materials and melt that forms after the coal seam has completely combusted (Heffern et al., 2007; Figure 2). An ash layer may occur below this collapsed zone, comprising the residuum from the burned coal bed as well as minerals precipitated by groundwater (Heffern et al., 2007). This ash is often powdery and gray, and is rarely exposed. The sediments immediately underlying the ash layer remain comparatively unchanged and show minimal signs of heating (Heffern & Coates, 2004).

Clinkers are more resistant to erosion and weathering than their host rocks and frequently occur as high relief features, such as butte tops and ridgelines. Paralavas are especially resistant and will protrude as “chimneys” high above the rest of the larger clinker outcrop (Grapes, 2010; Heffern & Coates, 2004; Roberts

et al., 1999). Clinker deposits often date within the last 5 Myr, with the oldest pyro-metamorphic rock dated at ~15 Myr in the Hatrurim Fm. in Israel (Ron & Kolodny, 1992). In the PRB in the United States, clinker ages span much of the Quaternary, with the oldest dated clinker material at 4 Myr (Heffern et al., 2007; Reiners et al., 2011; Riihimaki & Reiners, 2012; Riihimaki et al., 2009).

In this study, clinker samples were collected from Montana's Custer National Forest in the northern portion of the PRB (Figure 1; Table S1). The PRB is a sedimentary basin in NE Wyoming and SE Montana (Luppens et al., 2015) formed during the eastward progression of the Laramide Orogeny. The basin contains the thick lacustrine and fluvial deposits of the Paleocene Fort Union Formation and the overlying Eocene Wasatch Formation, the latter being absent throughout most of the Montana PRB including deposits in Custer National Forest (Luppens et al., 2015). The basin is home to one of the world's most productive sub-bituminous coal reserves, most of which occurs in the upper and lower members of the Fort Union Formation (Flores & Bader, 1999). Erosional downcutting throughout the Quaternary and, more recently, removal of overburden for mining, has exposed many of these coal beds, making them susceptible to ignition (Heffern & Coates, 2004). An estimated 4,500 km² of the 50,500 km² PRB have been affected by coal fires as evidenced by extensive clinker deposits exposed throughout the basin (Luppens et al., 2015).

The geology in the Custer National Forest is dominated by fluvial sediments of the Tongue River Member of the Fort Union Formation. These late Paleocene sediments (~60 Ma) represent both floodplain (coal, shale, mudstone, siltstone, and fine sandstone) and channel (medium-coarse sandstone) depositional environments (Belt et al., 2004). The sandstones are dominantly litharenites that captured sediment eroding from the uplift of the Bighorn mountains to the East, comprising material from carbonate, metamorphic, and crystalline rocks (Whipkey et al., 1991). The clinkers within the Custer National Forest are often associated with the Wyodak-Anderson and Knobloch coal zones of the Tongue River Member, but may also be associated with minor coal seams that lie between these two zones (Heffern & Coates, 2004). Clinkers occur up to several meters in thickness and commonly crop out at the top of buttes. Thinner, weakly baked deposits may be associated with minor coals and occur in the middle of buttes. However, these deposits generally have not undergone enough heating to transform the primary sedimentary deposits into the clinker lithologies as defined above, and as such we differentiate them here by categorizing these deposits as weakly baked sediments. In some locations, clinkers can be traced back to outcrops where the coal seam has not been burnt, indicating more recent coal fires or areas recently exposed by erosion. The clinker deposits in this region have been extensively mapped by Heffern et al. (2013) and many have been dated using fission track and (U-Th)/He geochronology (Heffern et al., 2007; Reiners et al., 2011; Riihimaki & Reiners, 2012; Riihimaki et al., 2009). Clinker ages in this region range from 7 ± 6 ka (all uncertainties reported at 2σ) to 1.11 ± 0.04 Ma (Heffern et al., 2007; Reiners et al., 2011; Riihimaki & Reiners, 2012; Riihimaki et al., 2009). Jones et al. (1984) conducted preliminary paleomagnetic investigations on clinkers from this area, including rock magnetic and paleodirectional assessments, and found that characteristic remanent magnetizations were consistent with the expected paleofield direction at the time of clinker formation (Jones et al., 1984).

3. Materials and Methods

3.1. Sampling

Samples for rock magnetic analyses were collected from eight clinker deposits in the Tongue River Member of the Fort Union Formation: one from the burnt Wyodak-Anderson coal zone, one from the burnt Knobloch coal zone, and six from burnt coal seams between the Knobloch and Wyodak-Anderson coal zones. Sampled materials include paralavas, unbaked sediments (dominantly siltstones), weakly baked sediments (dominantly siltstones and mudstones), baked fine-grained sandstones, baked siltstones, and porcellanite, in addition to pyro-metamorphic breccias and coal ashes. Some samples contain both baked and melted material, with melted material forming bands of darker color. Oriented samples were collected from baked sediments and paralavas, as these were the most consolidated. Unbaked and weakly baked material was not well lithified, and for this study, unoriented, largely disaggregated sediment powders were collected from these areas. A number of unoriented samples were also collected to maximize the diversity of clinker products studied, including various textures, colors, and lithologies. Profiles through two well-exposed clinker outcrops were collected. Profile CNFP3 sampled an undated clinker deposit (Undated-1) extending from 2 m below a burned coal horizon up to the top of the clinker, ~8 m above. This clinker caps the butte

and no material exists above it. Profile CNFP6 sampled an undated, weakly baked clinker deposit (Undated-2), where the coal seam was not completely combusted. This clinker is under- and overlain by unbaked sediments and samples were collected from the base of the burnt coal seam to ~5.4 m above the weakly baked material. For this study, only unoriented samples were collected in each profile.

One-inch cores were cut from the oriented block samples using a drill press and a double bladed saw. Strongly baked profile chip samples were cut into four 1 cm³ cubes; weakly baked and unbaked profile powder samples were gently disaggregated with a mortar and pestle, mixed with PVA glue, and allowed to cure in 8 cm³ plastic boxes. Additionally, chips from both oriented and unoriented samples and were used to collect low-*T* data, hysteresis loops, first-order-reversal curve (FORC) diagrams, and to create powders for high-temperature (HT) susceptibility experiments.

3.2. Rock Magnetic Analyses

Frequency dependence of susceptibility (χ_{fd}) was measured using a MAGNON variable frequency susceptibility meter. Low (200 Hz) and high (2,000 Hz) frequency susceptibility were measured in a 300 Am⁻¹ applied field. Values are reported as percentages, where $\chi_{fd\%} = [(\chi_{200} - \chi_{2,000})/\chi_{200}] \times 100$.

HT low-field susceptibility experiments ($k(T)$) were conducted with a Geofyzika KLY-2 KappaBridge AC Susceptibility Bridge with CS2 furnace attachment using an AC field of 300 Am⁻¹ and a frequency of 920 Hz. Measurements were collected upon warming and cooling, with a peak temperature of 700°C. A single specimen was heated to 720°C. Initial experiments were conducted in an argon atmosphere. If an increase in susceptibility was observed upon cooling, replicate specimens were run in air. Replicates of five specimens were subjected to multiple heating and cooling cycles to estimate the temperature at which alteration occurred. Néel/Curie temperatures were determined by identifying negative peaks in the first derivative of the measured data and are only reported for samples with relatively reversible heating and cooling curves.

To assess the remanence properties of the samples, a series of laboratory magnetizations were induced and then demagnetized using alternating field (AF) methods. Anhyseretic remanent magnetizations (ARMs) were imparted in a peak AF of 170 mT with a DC bias field of 50 μ T. Next, samples were subjected to a progressive 10-step AF demagnetization sequence along the X, Y, and Z specimen coordinates with a peak field strength of 170 mT. These data provide a rough estimate of the remanence contribution of minerals with coercivities >170 mT, while also assessing the demagnetization behavior of grains with coercivities <170 mT. To look only at the remanence imparted by the ARM, we calculated the vector difference sum (VDS) demagnetization spectra for each specimen from 0 to 170 mT and normalized the magnetization from 0 to 1. Median destructive fields (MDFs) were calculated from these VDS demagnetization spectra. To assess the percentage of remanence remaining after demagnetizing to 170 mT, the remanence remaining after the 170 mT step was added back to the VDS of each demagnetization step for each demagnetization spectra. These values were then normalized. The magnitude of the y-component of magnetization at 170 mT multiplied by 100 marks the percentage of remanence remaining after the 170 mT demagnetization step, which we denote here as the parameter %HC, or percent high-coercivity. Note, this experiment was performed on profile samples which includes strongly baked unoriented chips (that were cut into cubes) and weakly baked and unbaked loosely consolidated sediment samples which were disaggregated and mixed with thinned, low viscosity glue. For the strongly baked cubes, this experiment assesses the natural remanence magnetization (NRM) contribution of minerals with coercivities >170 mT. For the weakly baked and unbaked materials, instead, these rough estimates of the contribution of high-coercivity remanence are of a laboratory depositional remanent magnetization (DRM), which may have a different efficiency than the original NRMs. As such, for weakly baked and unbaked samples, %HC values should be treated as minimum estimates of the high-coercivity remanence contribution. Note, also that because the unbaked and weakly baked sediment were collected as powders, NRMs could not be measured before imparting ARMs.

Hysteresis loops, backfield curves, and isothermal remanent magnetization (IRM) acquisition curves were measured on two MicroMag Princeton Measurements Vibrating Sample Magnetometers, with nominal sensitivities of 10⁻⁷ Am² and 5 \times 10⁻⁹ Am², respectively, using a maximum applied field of 1.5 T. All backfield curves and IRM acquisition curves were measured at room temperature. Major hysteresis loops were collected for most specimens at room temperature. Hysteresis loops were collected as a function of

temperature for a small selection of specimens in a helium atmosphere, beginning at room temperature and increasing in 25°C steps to a maximum temperature of 700°C. FORCs were collected from all representative clinker lithologies using an irregular grid and processed using iFORC (Zhao et al., 2017). Additional FORCs were collected from a subset of four representative specimens as a function of temperature. FORCs were measured pre-heating at room temperature, at 250°C, and again at room temperature post-heating, using a uniform grid. FORC data collected as a function of temperature were processed using FORCinel (Harrison & Feinberg, 2008).

Low-temperature experiments were performed on two Quantum Design Magnetic Properties Measurement Systems (MPMS-5S and MPMS-XL). We utilized the same protocols as Sprain et al. (2016). Both protocols used an applied field of 2.5 T and measurements were taken every 5 K between 20 and 300 K.

To better understand the mineralogy and range of coercivities present in clinker materials, a triaxial-TRM modified Lowrie experiment was performed (Lowrie, 1990). Three orthogonal TRM's were imparted sequentially using a 60 μ T bias field and an ASC Model TD-48SC Thermal Demagnetizer with a TRM field coil on specimens in following order: (a) full TRM from 700°C along +Z; (b) partial thermal remanent magnetization (pTRM) 600 to 20°C along +X; (c) pTRM 300 to 20°C along +Y. Samples were then stepwise demagnetized using a 70-step AF sequence with a peak AF step of 170 mT. Samples were measured and AF steps were performed on a 2G LongCore superconducting magnetometer with nominal sensitivity of 10^{-11} Am² inside a magnetically shielded room with background fields ≤ 200 nT.

4. Results

To highlight the observed variations in magnetic properties as a function of lithology, distance from the coal seam, oxidation state, and location, we organized our results section into four parts. The first part compares observed differences between measured lithologies: unbaked sediment, weakly baked sediment, strongly baked sediment (which we also refer to as baked sediment), porcellanite, and paralava. Most collected unbaked samples were siltstones and as such, we grouped them together. We present results in the order of increasing temperature of formation. As an approximate measure of oxidation state, we next report magnetic properties as a function of color, where darker colors (black and purple) are associated with reducing conditions, lighter colors (red and orange) are associated with oxidizing environments, and yellow indicates unbaked sediments. We next describe our results for each measured profile, highlighting observed magnetic changes as a function of distance from the burnt coal seam. Finally, we report observed differences between clinkers collected across the region, in addition to assessing variances between clinkers formed from different coal zones. All rock magnetic results are reported in Table S1 and plotted in Figures S1–S11 (found in Supporting Information S1). Raw measurement data can also be found on the MagIC database (Sprain et al., 2021).

4.1. Lithology

4.1.1. Unbaked Sediment

Unbaked sediment samples underwent ARM demagnetization, hysteresis, HT hysteresis, and HT and frequency dependent susceptibility analyses. We observe low saturation magnetization, remanent magnetization, and coercivity values, including small %HC values and moderate MDF values, in addition to low Curie points. Results from these experiments indicate that unbaked sediments contain one principal magnetic mineral: (titano)magnetite (and possibly intermediate titanohematite).

Hysteresis results on the one measured sample are consistent with the presence of a soft ferrimagnetic mineral (Figures S1A and 3). ARM demagnetization experiments show that unbaked samples have a relatively narrow %HC range of $\sim 2\%$ – 20% with a median of 7%, consistent with hysteresis results showing that the unbaked material does not have a strong high-coercivity component (Figures S2E and 4). The median MDF of the VDS demagnetization spectra estimated from these experiments is 32 mT (Figure S2H), further supporting the presence of a soft ferrimagnetic component. HT hysteresis analysis indicates that above 250–325°C, the samples exhibit only diamagnetic behavior, suggesting that remanence is held by a mineral with low Curie temperatures, consistent with titanomagnetite (Figure S3A). This result is corroborated by

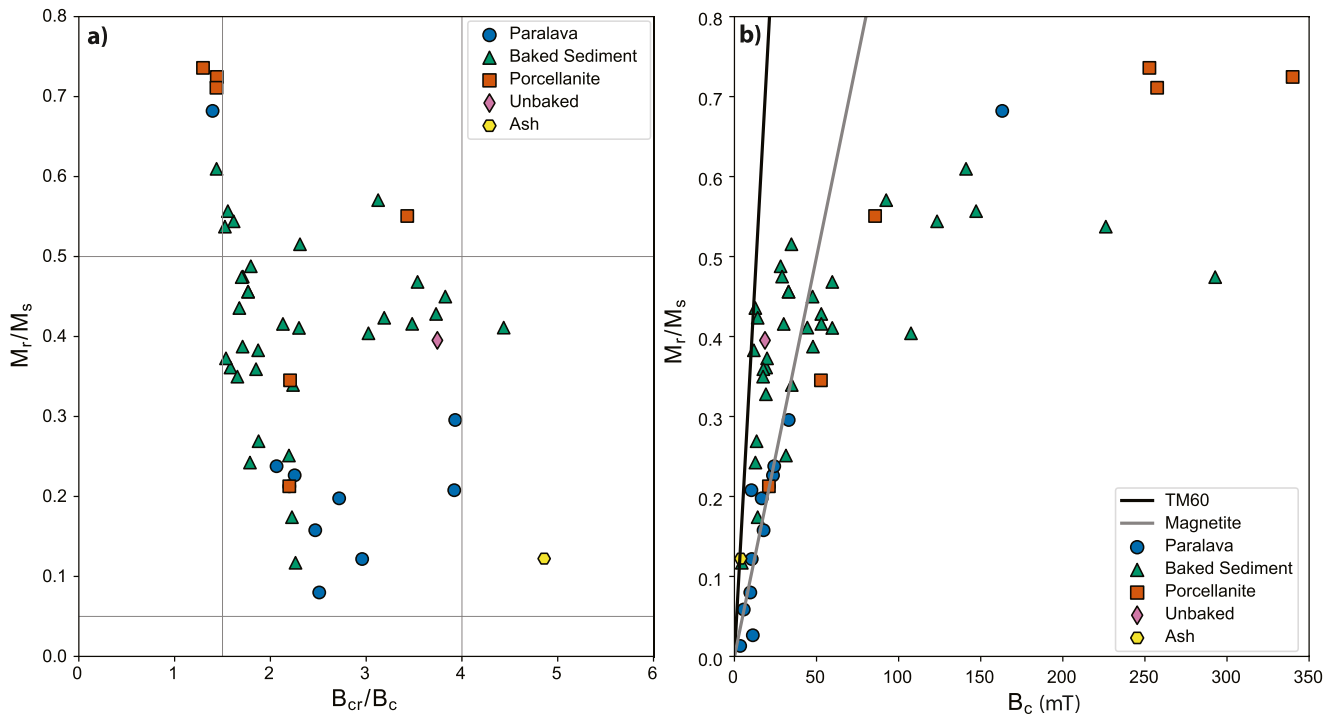


Figure 3. (a) Day plot of hysteresis ratios (M_r/M_s vs. B_{cr}/B_c) for measured clinker specimens (Day et al., 1977). (b) Squareness versus coercivity plot (M_r/M_s vs. B_c) for measured clinker specimens (Néel, 1955; Tauxe et al., 2002). Black and gray lines show trends for TM60 and pure magnetite after Wang and Van der Voo (2004). In both plots, color/symbol indicates different lithology types. M_r is saturation remanence, M_s is saturation magnetization, B_{cr} is coercivity of remanence, and B_c is coercivity.

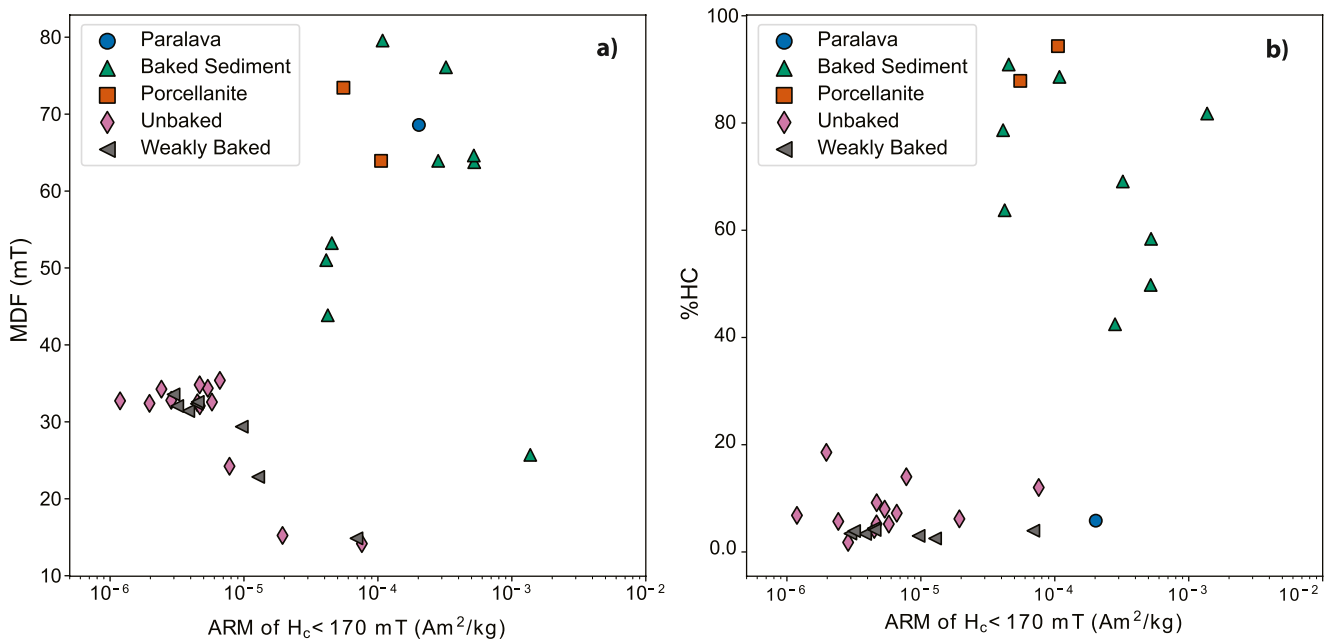


Figure 4. Results from anhysteretic remanent magnetization (ARM) demagnetization. (a) Median destructive field (MDF) calculated from the vector difference sum demagnetization spectra versus ARM after subtracting the remanence remaining after demagnetization to 170 mT. (b) Percent high-coercivity (%HC) versus ARM after subtracting the remanence remaining after demagnetization to 170 mT. In both plots, color/symbols shows lithology.

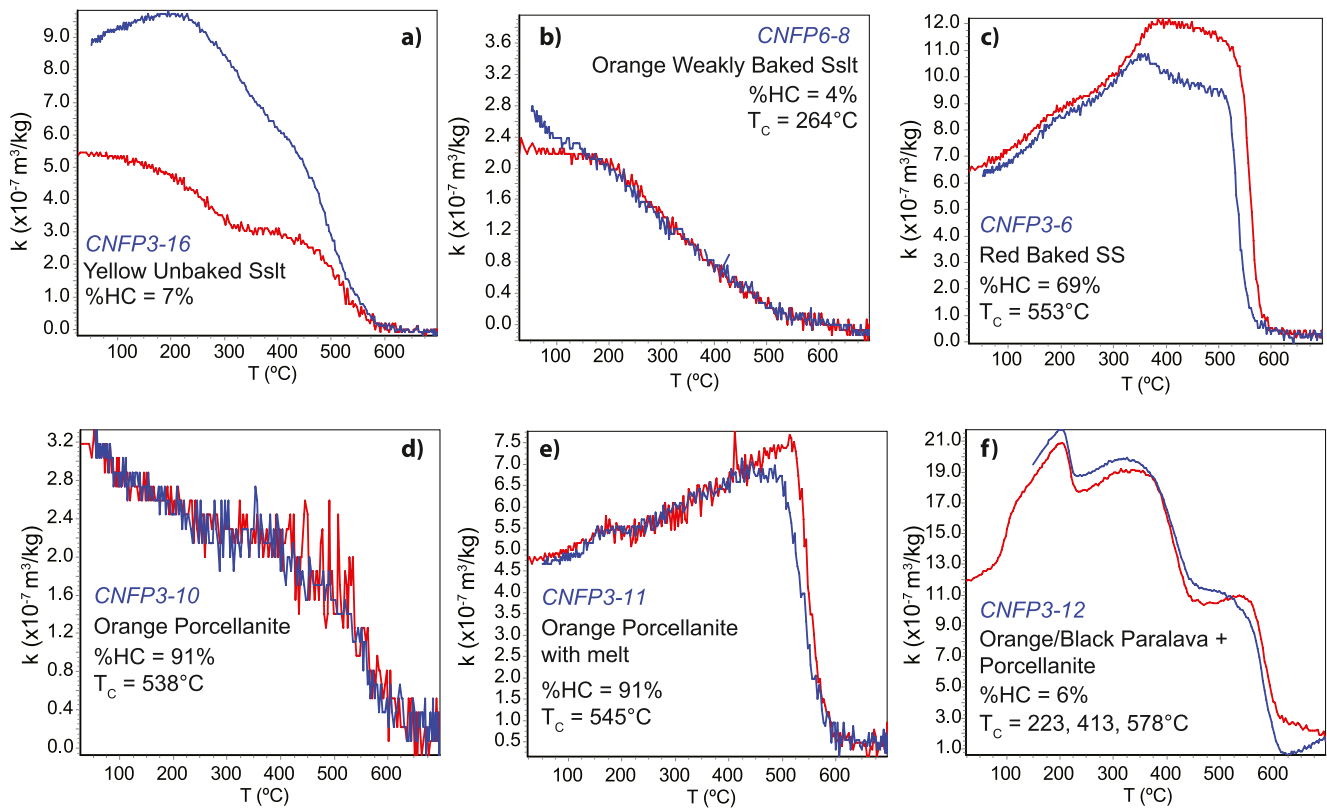


Figure 5. High-temperature heating (red) and cooling (blue) of bulk magnetic susceptibility in air for representative lithologies (a–e), and (f) CNFP3-12, which was measured in Ar. Néel/Curie temperatures (T_c) are indicated for samples that did not significantly alter in addition to median percent high-coercivity (%HC) values for each lithology group.

$k(T)$ experiments which identified Curie points $\sim 300^\circ\text{C}$ (Figures 5a, S4E and S4F). Additional drops in susceptibility were identified between 505 and 580°C (Figures 5a and S4A–S4J), however for most samples, these drops were accompanied by a large increase in susceptibility upon cooling and as such we attribute these phases to alteration. The $k(T)$ experiments conducted in an argon atmosphere resulted in an increase in susceptibility upon heating in all specimens (Figures S4A, S4B, S4D, S4E, S4G and S4I). For one specimen (CNFP3-16, Figure S4E), cyclic heating up to 700°C was performed in an Ar atmosphere. Data from this experiment show that alteration did not occur until $>400^\circ\text{C}$, and as such the low-temperature Curie point for this specimen ($\sim 300^\circ\text{C}$) is likely representative of a primary mineralogy. In air, the alteration was persistent for all but two samples (CNFP3-17 and CNFP6-14; Figures S4F and S4J). The creation of partially oxidized magnetite during heating of unbaked sediment in air and magnetite in argon suggests that this phase will likely exist in both oxidized and reduced clinker deposits.

Although the most likely magnetic mineral in the unbaked sediment samples is titanomagnetite, without a self-reversal test, we cannot eliminate the possibility that intermediate titanohematite is also present. Intermediate titanohematite shares many properties with titanomagnetite and has been found in similarly aged sediments in the nearby Hell Creek region, NE Montana (Sprain et al., 2016). Further experiments are necessary to check for the presence of this phase in unbaked material. Starting ARM values for unbaked sediment are the lowest of all measured lithologies, with values $\sim 1 \times 10^{-6}$ – 8×10^{-5} Am^2/kg (Figure 4).

4.1.2. Weakly Baked Sediments

Weakly baked sediment samples underwent ARM demagnetization experiments, frequency dependent susceptibility experiments, and HT susceptibility was measured for two specimens. We observe small %HC values, low MDFs, and susceptibility loss between 200 and 550°C . ARM demagnetization experiments reveal that weakly baked samples have the narrowest %HC range $\sim 2\%$ – 10% with a median of 4% (Figures 4

and S2E). In general, our observations suggest that weakly baked sediments contain primarily two magnetic mineralogies: titanomagnetite and hematite.

The median MDF from the VDS demagnetization spectra for weakly baked sediment is ~ 32 mT (Figure S2H), suggesting that grains with coercivities < 170 mT are a soft ferrimagnetic phase similar to that of our unbaked samples. For the two specimens that underwent $k(T)$ experimentation in air, one showed reversible behavior between heating and cooling, but did not have a distinct Curie point and instead gradually lost susceptibility between 200 and 550°C (Figure 5b). The observed reversible behavior suggests that baking, as result of the coal fire, helped to stabilize its magnetic mineralogy in air. The other specimen (CNFP6-1) that went under $k(T)$ experimentation did show minor alteration, but less than the unbaked specimens (Figure S4K). No weakly baked specimens were run with an Ar atmosphere. Evidence of a soft magnetic phase, in combination with susceptibility loss at low temperatures, lead us to assign this phase to titanomagnetite.

Evidence for hematite includes the possible remaining susceptibility above 600°C in $k(T)$ experiments and the red/orange color of the specimens. For specimen CNFP6-8 that had reversible behavior during $k(T)$ measurement, a small portion of the original susceptibility remained after heating to 585°C and was totally removed by 700°C (Figure 5b), suggesting that this specimen may contain some hematite. Further, the distinct red/orange color of many of the weakly baked specimens suggests that oxidation occurred and that hematite may exist. The low %HC values suggest that this phase, if present, is not contributing significantly to the laboratory-induced DRM, but may contribute more strongly to the NRM. ARM starting values for weakly baked samples are around 3×10^{-6} – 7×10^{-5} Am²/kg, and on average are slightly higher than those for unbaked sediment, suggestive of the formation of new magnetic material (Figure 4).

4.1.3. Strongly Baked Sediment and Porcellanite

Strongly baked sediment samples underwent ARM demagnetization, high-frequency and HT susceptibility, hysteresis, HT hysteresis, modified Lowrie, FORC analysis, and low- T experiments. Results from these experiments suggest that strongly baked sediments contain varying proportions of two principal magnetic minerals: a high-coercivity, thermally stable, low unblocking temperature phase (HCSLT) and (titano)magnetite, with minor contributions from intermediate titanohematite and hematite. Porcellanite samples underwent similar experiments and their results suggest that these samples also contain varying proportions of a HCSLT phase and (titano)magnetite, with minor contributions from hematite.

Several lines of evidence point to the presence of a HCSLT phase: hysteresis loops with hysteresis shape parameter (σ) values greater than zero, high %HC values, a large increase in room-temperature saturation isothermal remanence (RTSIRM) on cooling, significant drops in magnetization at 150–225°C, a magnetically hard, low unblocking temperature phase in the modified Lowrie tests, and distinct high-coercivity peaks observed in FORC analysis that disappear by 250°C. A majority of the measured hysteresis loops have σ values greater than zero, ranging from ~ -0.1 to 0.8 for strongly baked sediment and -0.1 to 0.4 for porcellanite, correlating to varying proportions of both hard and soft magnetic phases (Figures 6a–6c, S1B–S1JJ and S2G). σ , is a measure of hysteresis shape and compares the actual area of the curve, E_{hys} , to a rectangular area with a height and width defined by $2M_s$ and $2B_c$, respectively (Fabian, 2003). It is defined by the following equation:

$$\sigma = \log \left(\frac{E_{\text{hys}}}{4M_s B_c} \right). \quad (1)$$

Log represents the natural logarithm. Values greater than zero are obtained for loops that are traditionally referred to as “wasp-waisted” or “goose-necked,” and values less than one to loops commonly referred to a “pot-bellied.” Here, we believe the magnetically hard phase to be correlated to our HCSLT phase, supported by our other analyses. IRM and backfield curves are consistent and show an unsaturated high-coercivity tail in a majority of samples (Figures S1B–S1JJ). Plotting the data on Day (Day et al., 1977) and squareness versus coercivity (M_r/M_s vs. B_c ; Néel, 1955; Tauxe et al., 2002) plots further highlights the presence of this high-coercivity phase (Figure 3). Additionally, the hysteresis data suggest that the high-coercivity phase is unlikely to be hematite, which could not explain the large magnetizations associated with the strongly baked sediment and porcellanite samples. Hysteresis results are further corroborated by ARM demagnetization experiments, which reveal that these clinker lithologies have a significant portion of their remanence

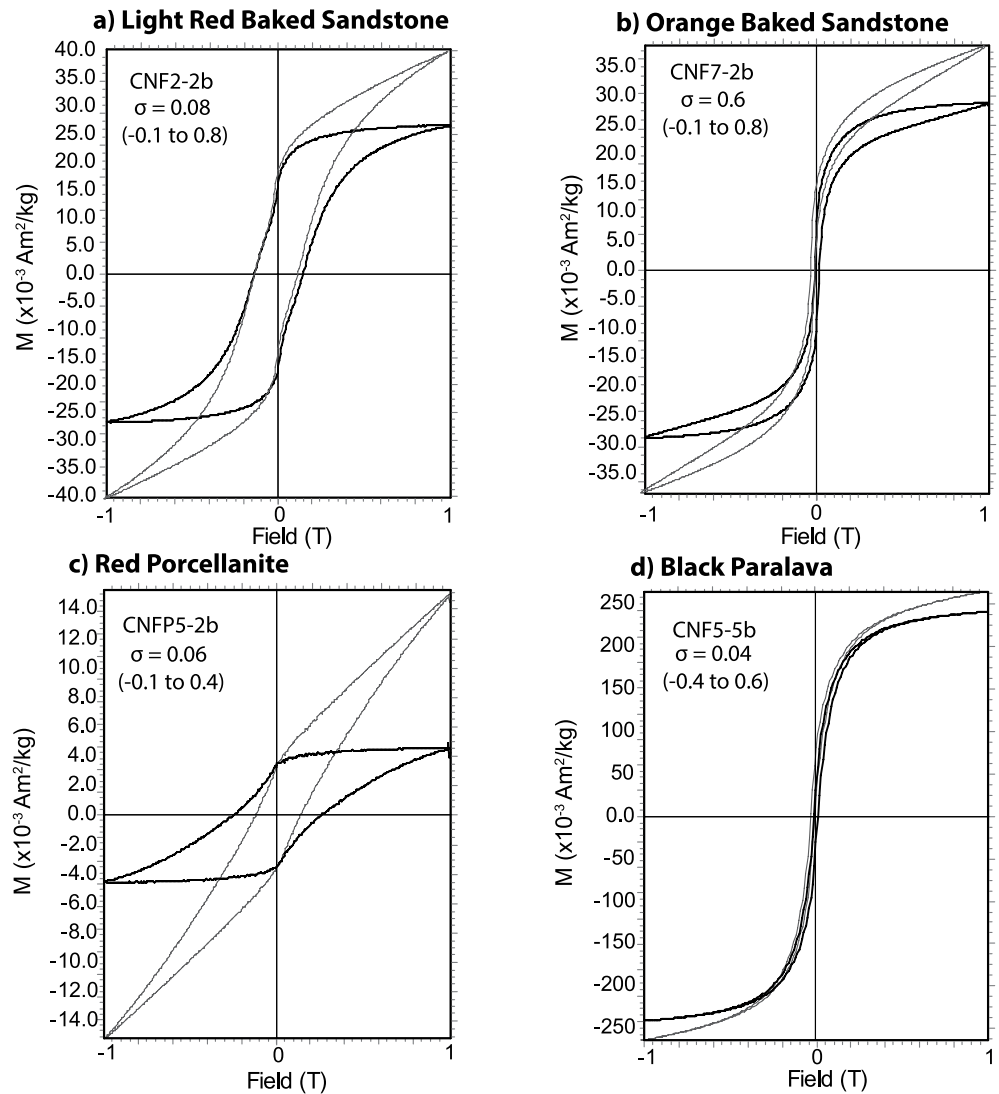


Figure 6. Representative hysteresis loops for different clinker lithology types (a–d). In each case, the black curve is the slope-corrected loop and gray is uncorrected. M is magnetization and Field is applied field. σ values are shown for each loop and the range of σ values for each lithology type are shown in parentheses.

held by a high-coercivity phase, with %HC values ranging ~45%–95% with a median of 69% for strongly baked sediment samples, and %HC values ~88%–95% with a median of 91% for porcellanite samples (Figures 4 and S2E).

Low-temperature magnetometry experiments display two dominant behaviors that are consistent with the presence of two main magnetic phases for most samples (Figures 7a–7c and S5A–S5MM). In ~50% of samples, RTSIRM curves show a large increase (~30%–100%) in remanence on cooling, suggestive of a magnetic mineral with a low ordering temperature (Figures S5A, S5B, S5E, S5F, S5M–S5O, S5R–S5V, S5GG, S5JJ and S5LL). The lack of a wide-spread between field-cooled (FC) and zero-field cooled (ZFC) remanences (FC is less than twice ZFC) in these samples indicates that this phase is not likely to be goethite (e.g., Dekkers, 1989; France & Oldfield, 2000; Lowrie & Heller, 1982; Strauss et al., 2013). Instead, we believe this behavior is connected to the HCSLT phase, which is supported by our HT hysteresis analysis. HT hysteresis experiments show evidence of three distinct magnetic minerals (Figures 8 and S3B–S3F). The HCSLT phase in these experiments is marked by a distinct drop in M_s , M_r , and B_c by 225°C, with derived Curie points ~150–225°C, suggesting that the previously described low- T behavior is attributable to the HCSLT phase. Further, these results suggest that the high-coercivity, high-magnetization component identified in

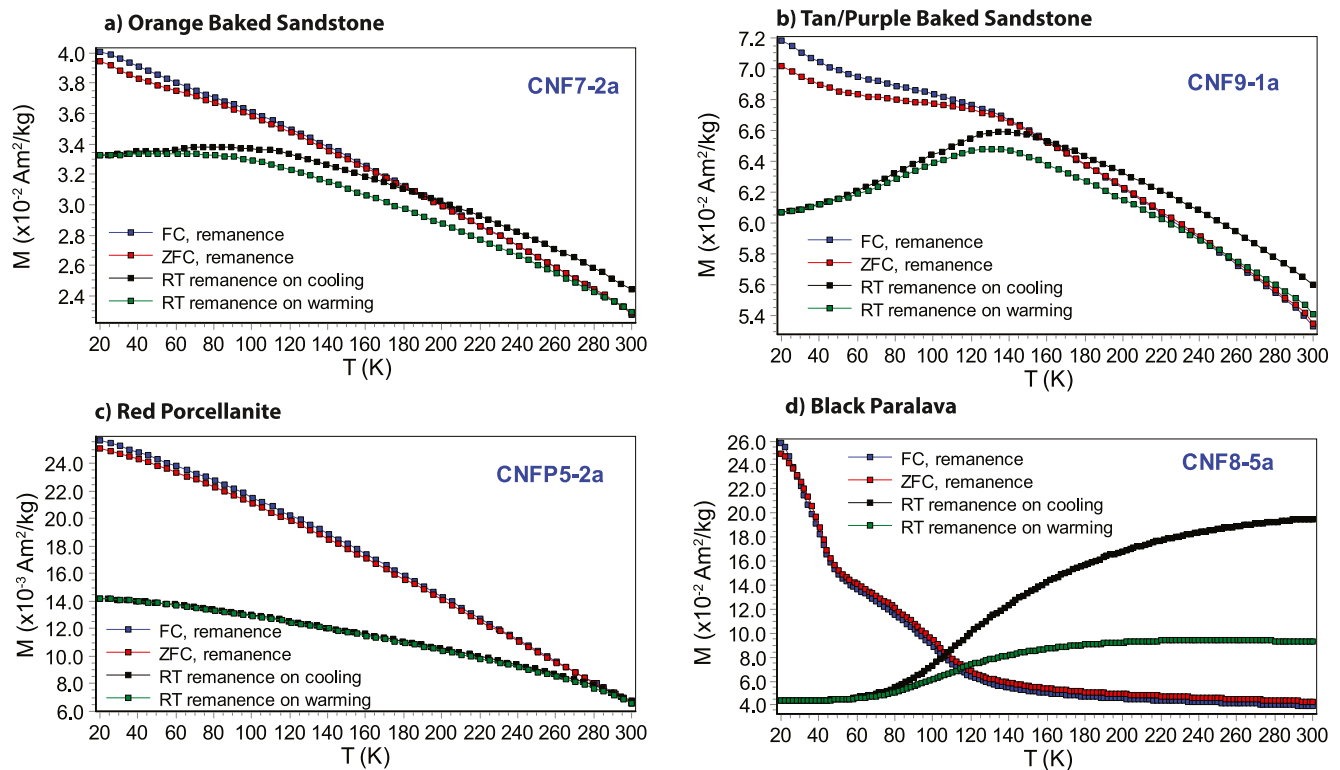


Figure 7. Low-temperature magnetization curves on clinker specimens for representative clinker lithologies (a–d). Plots show measurements of magnetization (M) during cooling (black) and warming (green) following the application of a saturation isothermal remanent magnetization (SIRM) applied at room temperature (RT) in addition to measurements of magnetization during warming. Following a sustained direct current field of 2.5 T during cooling (field-cooled, FC: blue), and measurements of magnetization during warming following a SIRM imparted at low temperature (zero field-cooled, ZFC: red).

room-temperature hysteresis analysis and ARM demagnetization experiments has a low Curie temperature and is attributable to the HCSLT phase. Additionally, above 225°C, for some samples hysteresis curves transitioned from having σ values greater than zero to values closer to zero (Figures 8 and S3E) demonstrating that one of the magnetically hard phases contributing to the observed hysteresis behavior with large σ values is the HCSLT phase. Evidence for the HCSLT phase was not clearly identified in $k(T)$ experiments, but may be attributed to a slight kink in the curves around 200°C (Figures 5c–5e), suggesting that this phase does not contribute significantly to the bulk susceptibility. It is important to note that 11/15 $k(T)$ curves measured in air were reasonably reversible (Figures 5c–5e, S4L, S4R, S4S, S4U, S4W, S4Y, S4GG and S4TT), suggesting that this mineral is thermally stable.

Results from the modified Lowrie test further indicate the presence of a high-coercivity, low-unblocking temperature phase. Note, no porcellanite samples were run in this experiment. For a majority of specimens, the TRM is held by both hard low ($T_{ub} < 300^\circ\text{C}$) and soft mid unblocking temperature ($300^\circ\text{C} < T_{ub} < 600^\circ\text{C}$) phases, in varying proportions (Figures 9a–9c and S6A–S6C). The low T_{ub} phase ranges in its contribution to remanence (making up small to large portions of the total remanence) and is not removed by AF fields of 170 mT, consistent with the HCSLT phase (Figures 9a, 9c, S6A and S6B). FORC analysis additionally points to the presence of a high-coercivity phase, with high-coercivity tails extending to ~100 to >200 mT for ~80% of measured samples (Figures 10a, S7A, S7D, S8B–S8E, S8H, S8J, S8K, S8M, S8N, S8P and S8Q). FORC diagrams measured at 250°C show a clear loss of these high-coercivity peak/tails, demonstrating that they are generated by the HCSLT phase (Figures 10b, S7B and S7E).

Evidence for (titano)magnetite include: hysteresis loops with σ values greater than zero, low- T transitions near ~120K, Curie points ~530–575°C, a magnetically soft, high unblocking temperature phase in the modified Lowrie tests, and strong coercivity peaks around 5–20 mT observed in FORC analysis that remain at 250°C. As previously mentioned, a majority of the measured hysteresis loops had σ values greater than zero (Figures 6a–6c, S1B–S1JJ and S2G). We believe the magnetically soft phase is best attributed

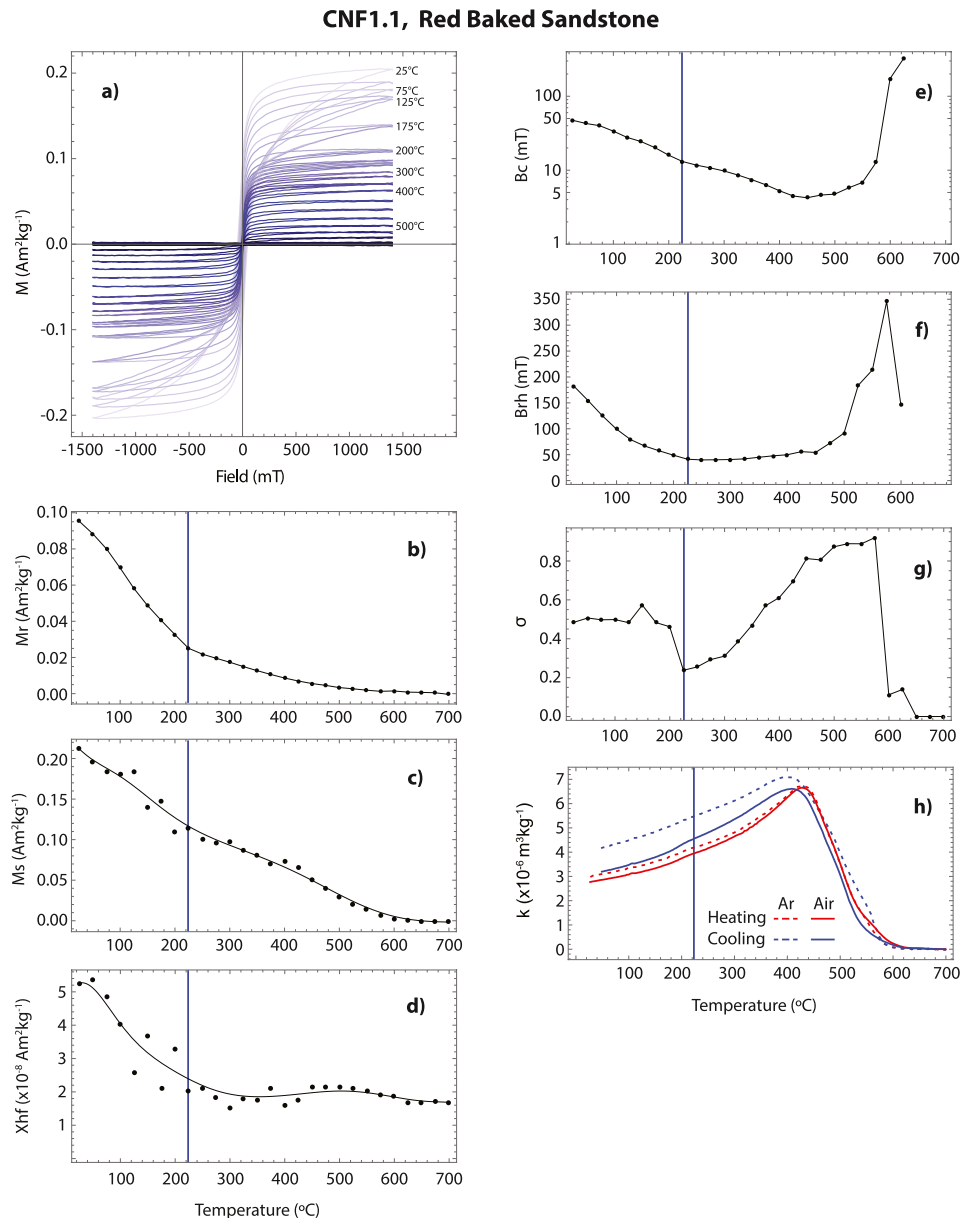


Figure 8. Temperature dependence of hysteresis and low field susceptibility for specimen CNF1.1. Vertical blue line at 225°C marks inflection in M_r , B_c , and σ associated with Curie temperatures of ϵ -Fe₂O₃. M is magnetization (a), M_r is saturation remanent magnetization (b), M_s is saturation magnetization (c), χ_{hf} is high-field susceptibility (d), B_c is coercivity (e), B_{rh} is an estimate of remanent coercivity measured from the hysteresis loop (f; von Dobeneck, 1996), σ is the calculated hysteresis shape parameter value (g), and k is susceptibility (h).

to (titano)magnetite. The soft phase is also identified in our ARM demagnetization experiments, which yielded median MDF values of ~ 67 mT for strongly baked sediment samples and ~ 67 mT for porcellanite samples, more than twice that measured in weakly baked or unbaked sediment (Figures 4 and S2H).

In addition to the large increase in RTSIRM on cooling in our low- T experiments, $\sim 40\%$ of the strongly baked sediment and porcellanite samples showed evidence of isotropic points ~ 120 K, consistent with the presence of (titano)magnetite/maghemite (Figures 7a, 7b, S5I–S5L, S5N, S5R, S5CC, S5EE, S5HH and S5JJ; Church et al., 2011; Moskowitz et al., 1998). For all samples, the transition is smeared out across a broader temperature range compared to standard Verwey transition, which suggests that the magnetite may be partially oxidized to maghemite. It is also important to note that in many samples this signal may be partially

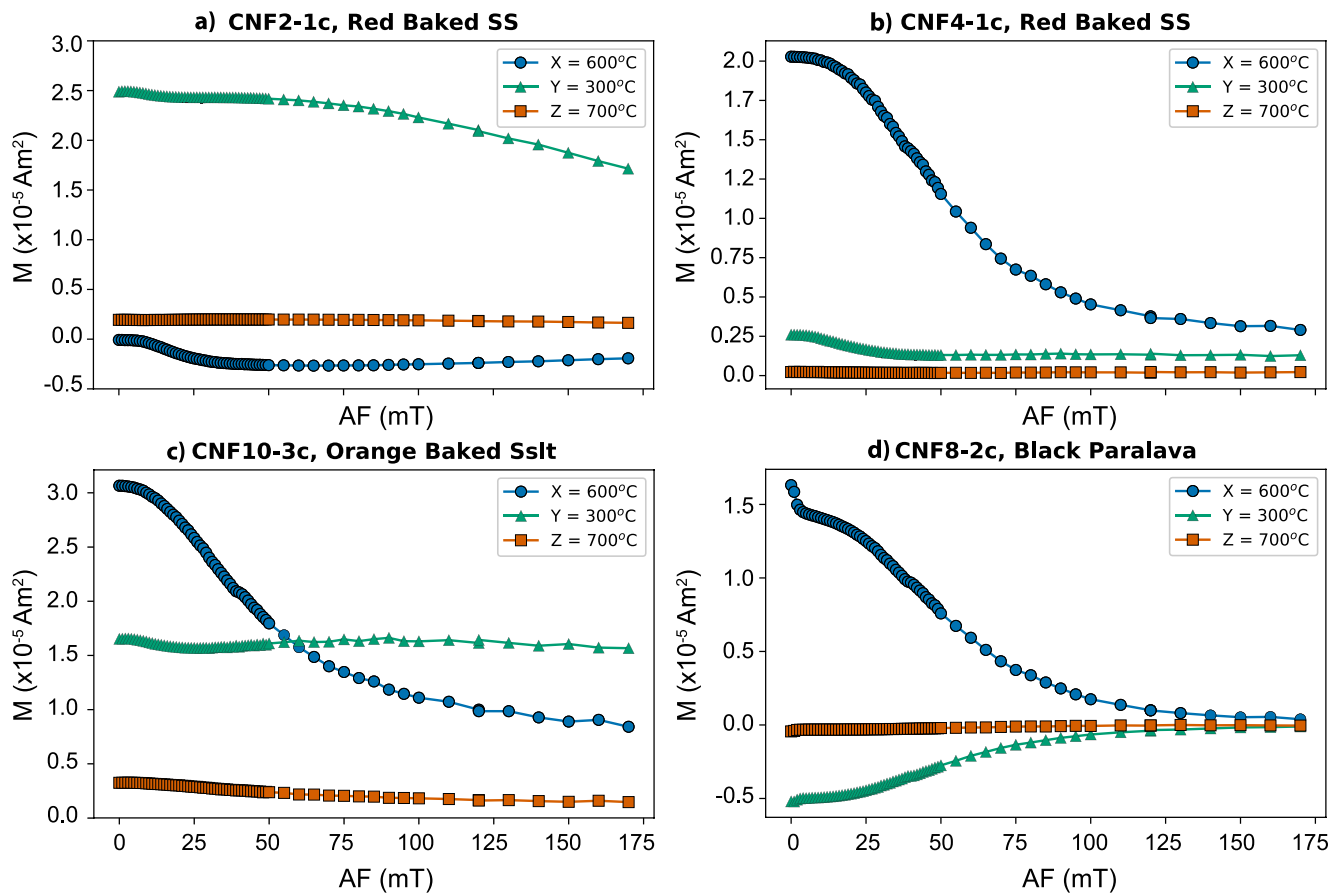


Figure 9. Alternating field demagnetization of thermal remanent magnetization (TRM) imparted along orthogonal X, Y, and Z axes for four representative clinker lithologies (a–d). M is magnetization and AF is applied alternating field. Approach is modified from that of Lowrie (1990).

obscured by that of the HCSLT phase. In HT hysteresis analysis, we see that this phase is most likely low-Ti magnetite, or a partially oxidized variant. The second phase identified in HT hysteresis experiments is associated with a continued drop in M_p , M_s , and B_c after heating above 225°C, with only <10% of the magnetization remaining after ~600°C (Figures 8 and S3B–S3F). Curie temperatures derived from these experiments for this component were generally ~500–575°C. These values are consistent with Curie points estimated from $k(T)$ experiments in air (~500–570°C) and point to the presence of low-Ti magnetite (Figures 5c–5e, S4L, S4R, S4S, S4U, S4W, S4Y, S4BB, S4DD, S4GG, S4II, S4NN, S4OO, S4SS and S4TT; Table S1). The $k(T)$ experiments conducted in an argon atmosphere resulted in an increase in susceptibility upon heating in all specimens except one (CNF1.1, Figure S4M), suggesting new strongly magnetic minerals were formed. For samples that were also run in air, this alteration did not persist (except for CNFP7-3; Figures S4LL and S4MM) and heating and cooling curves were close to reversible suggesting that the low-Ti magnetite phase is primary. Cooling curves for these specimens do tend to be lower in susceptibility than the heating curves (Figures S4S, S4U, S4W, S4Y, S4BB, S4DD, S4II and S4NN), suggestive of minor oxidation.

Results from the modified Lowrie test also point to the presence of low-Ti magnetite. The soft mid-unblocking temperature ($300^\circ\text{C} < T_{ub} < 600^\circ\text{C}$) phase in all but one sample (CNF2-1c) makes up a large portion of the total remanence (Figures 9b, 9c and S6A–S6C). The majority of this remanence is lost by AF fields of 150 mT, however, in most samples, upwards of ~30% of the remanence remains after demagnetization to 170 mT (Figures 9b, 9c and S6A–S6C). This behavior suggests that two phases of (titano)magnetite (or partially oxidized variants) may be present, possibly indicating different grain size populations, one with coercivities below 150 mT and one with high-coercivity values >170 mT. FORC analysis also points to the presence of a magnetically soft phase (Figures 10a, S7A, S7D and S8A–S8Q). The majority of measured FORC diagrams contain a coercivity peak around 5–40 mT with interaction fields (H_u) extending in both

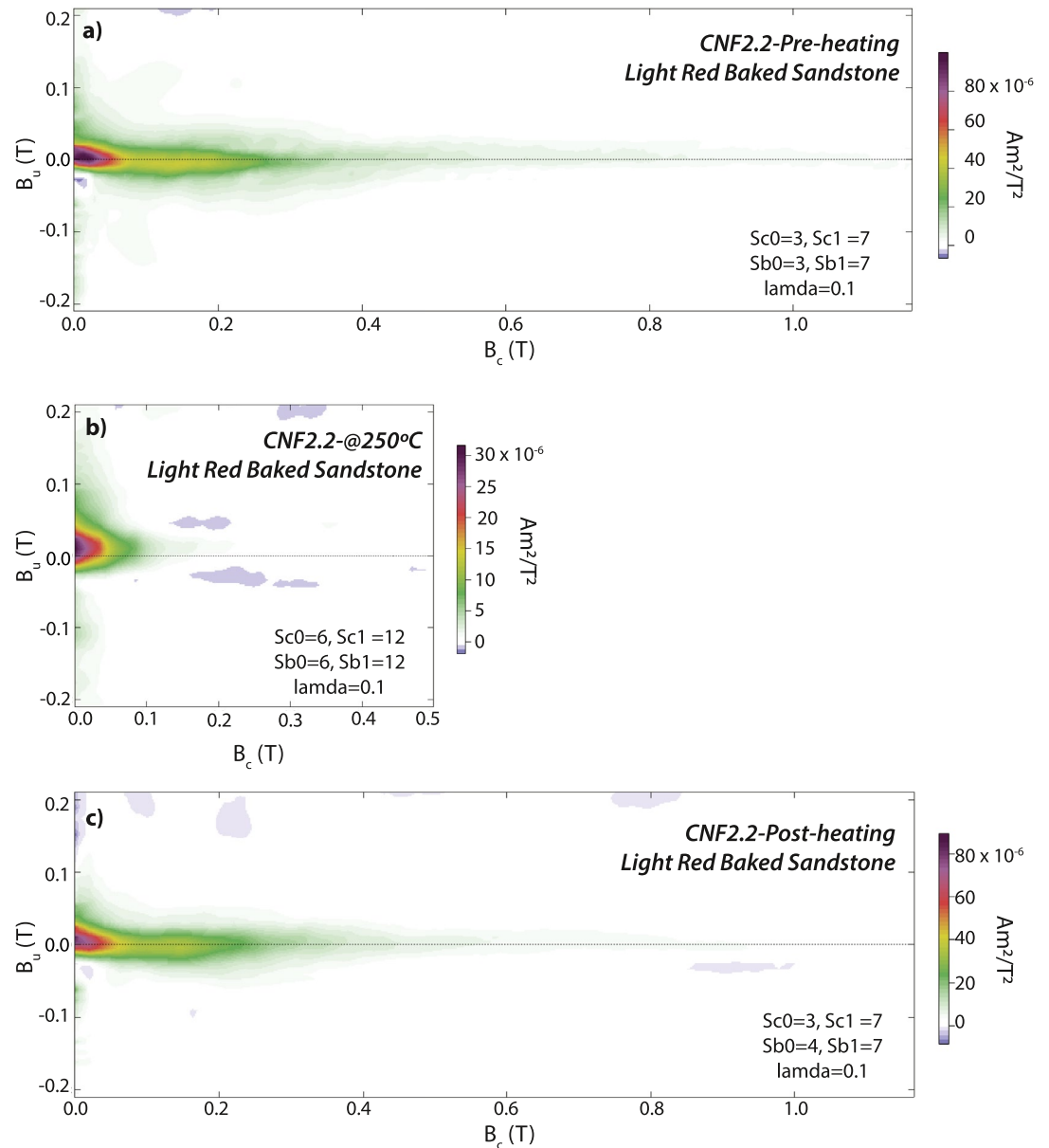


Figure 10. High-temperature first-order-reversal curve (FORC) distributions for one representative clinker sample. The distributions in panels (a) and (c) are the pre- and post-heating measurements at room temperature, while results in panel (b) were measured at 250°C. Distributions were calculated using FORCinel v.3.06 (Harrison & Feinberg, 2008) and the VARIFORC method of Egli (2013). Each FORC distribution was produced after subtracting an averaged lower branch and removing the first point artifact.

directions to $\pm 5\text{--}50$ mT (Figures 10, S7 and S8A–S8Q). The peak represents contributions from a vortex-like soft magnetic phase, likely magnetite. At 250°C, the FORC diagrams show a clear loss of the highest coercivity peak/tail, as previously mentioned, but the lower coercivity peak attributable to magnetite remained mostly unchanged with a slight shift to values below 5 mT (Figures 10b, S7B and S7E). Post-heating FORC diagrams are similar to pre-heating diagrams, but display a slight shift in the lower coercivity peak toward higher coercivity values, possibly indicative of minor alteration (Figures 10c, S7C and S7F).

In addition to the HCSLT and magnetite phases, our experiments also indicate that strongly baked sediments and porcellanites contain minor contributions from hematite and intermediate titanohematite. Evidence for hematite includes the presence of the Morin transition in low- T experiments, and high-coercivity,

high unblocking phase revealed in HT hysteresis experiments. In all of the low- T experiments, only one specimen displayed a possible Morin transition, suggestive of the presence of low-Ti hematite larger than $>0.1 \mu\text{m}$ (CNFP2-3; Figures S5W and S5X; Dunlop & Özdemir, 2001). Additionally, in the HT hysteresis experiments, after removal of the magnetite phase at 585°C , we can see that the hysteresis loops changed shapes and became dominated by a high-coercivity low- M_s phase, consistent with hematite (Figure 8). This is also marked by a rise in M_r/M_s and B_c starting around 600°C , which drops off by 700°C (Figures 8 and S3B–S3F). Although hematite is present, it does not contribute significantly to remanence, as the high unblocking phase ($T_{\text{ub}} > 600^\circ\text{C}$) in the modified Lowrie experiments holds very little remanence (Figures 9a–9c and S6A–S6C). Evidence for intermediate titanohematite in strongly baked sediments comes solely from the modified Lowrie test. Again, note, that no porcellanite samples were used in this experiment. In most specimens, the low T_{ub} phase ($<300^\circ\text{C}$) displays an initial drop in remanence that is then partially regained by AF fields of ~ 50 mT, suggesting that a phase with remanence antiparallel to the applied field is being removed (Figures 9a, 9c, S6A and S6C). This behavior is consistent with the presence of intermediate titanohematite, which has a Curie temperature of $\sim 300^\circ\text{C}$ and self-reverses upon application of a TRM (Fabian et al., 2011; Nagata, 1961; Nagata & Akimoto, 1956). This mineral has been identified in sediments from the Fort Union Fm. in the Hell Creek region of Montana (Sprain et al., 2016), and it is possible that this mineral was a part of the primary DRM of these sediments before clinker formation. We also see evidence for possible low Curie points in a few specimens, ~ 200 – 400°C , which may be attributable to this phase (Figures 5d, S4N, S4P, S4BB, S4OO and S4TT). Regardless of its presence, like hematite, this phase does not appear to be contributing significantly to remanence (Figures 9a, 9c, S6A and S6C).

The initial ARM for strongly baked lithologies ranges between 5×10^{-5} and $1 \times 10^{-3} \text{ Am}^2/\text{kg}$, which are clearly higher than weakly baked or unbaked samples, suggesting that these materials have a higher concentration of magnetic materials (Figure 4).

4.1.4. Paralava

Paralava samples underwent ARM demagnetization, high-frequency and HT susceptibility, hysteresis, HT hysteresis, modified Lowrie, FORC analysis, and low- T experiments. These experiments indicate that the primary magnetic mineral in paralava is magnetite/titanomagnetite, with contributions of the HCSLT phase in circumstances where small clasts of baked sediment were incorporated into the melt, in addition to minor contributions of intermediate titanohematite, hematite, and in one specimen, native Fe.

Evidence for (titano)magnetite includes: hysteresis loops consistent with a magnetically soft phase, low- T transitions near $\sim 120\text{K}$, Curie points ~ 520 – 580°C , a magnetically soft, high unblocking temperature phase in the modified Lowrie tests, and coercivity peaks around 20 mT observed in FORC analysis. Major hysteresis loops show a low-coercivity phase consistent with a soft ferrimagnetic mineral like magnetite (Figures 6d and S1KK–S1VV) and in rare cases a high-coercivity-high-magnetization phase consistent with the HCSLT phase, but we attribute this to clasts of baked sediment that have been incorporated in these samples (Figures S1MM, S1OO and S1PP). Most hysteresis loops are dominated by the low-coercivity phase, with higher room temperature saturation and remanent magnetization than baked sediments (Figure 3; Table S1). σ values range from -0.4 to 0.6 , with a median value around -0.1 , consistent with the interpretation that paralavas are dominated by a single magnetic phase (Figures 6d and S2G). IRM and backfield curves are also consistent with this trend and are mostly saturated by 1 T (Figures S1KK, S1LL, S1NN, S1QQ, S1RR, S1SS, S1TT and S1UU). Evidence for a soft magnetic phase is also observed in our ARM demagnetization experiments, which for the one sample analyzed (CNFP3-12) yielded a %HC value of 6%, considerably lower than porcellanite and strongly baked sediment samples (Figures 4 and S2E). The MDF calculated from the VDS demagnetization spectrum for this sample is 68 mT (Figures 4 and S2H).

Low-temperature magnetometry experiments show evidence of magnetite and/or titanomagnetite in all measured samples (Figures 7d and S5NN–S5SS). For these samples, a transition near 120 K was observed, indicative of the Verwey transition or low- T isotropic points. In some samples, this transition was clearly at 120 K (Figures 7d, S5PP and S5QQ), whereas for the others (Figures S5NN, S5OO, S5RR and S5SS) the transition occurred over a broader temperature range, indicative of partial oxidation (Church et al., 2011; Moskowitz et al., 1998). In general, compared to results from baked sediments and porcellanite, paralava samples displayed sharper low- T transitions suggesting a more stoichiometric magnetite component is present. HT hysteresis experiments show evidence for the presence of low-Ti magnetite, with estimated Curie

points $\sim 575^\circ\text{C}$ (Figure S3H). Curie points derived from $k(T)$ experiments corroborate this result and were generally between 510 and 520°C or $\sim 575^\circ\text{C}$ (Figures 5f, S4VV and S4WW; Table S1). All $k(T)$ experiments for paralavas were run in Ar atmospheres and heating and cooling curves are generally reversible (Figures 5f, S4VV and S4WW).

Two paralava samples were included in the modified Lowrie test. One was entirely composed of melt (CNF8-2c; Figure 9d) and the other contained an incorporated clast of baked sediment (CNF5-6c; Figure S6D). For the specimen entirely composed of melt, most of its remanence is held by the mid T_{ub} phase ($300^\circ\text{C} < T_{\text{ub}} < 600^\circ\text{C}$) and its remanence is almost entirely removed by AF fields of 170 T (Figure 9d). The room temperature FORC distributions for paralavas without blocks of clinker sediment exhibit well-developed central ridges with coercivity peaks around 10 – 60 mT and are differentiated from the strongly baked sediments and porcellanite by greater interaction fields (Figures S8S and S8U–S8Y). This behavior is generally indicative of vortex-like grain sizes.

Paralava samples with incorporated blocks of baked material show evidence for the HCSLT phase including: wasp-waisted hysteresis loops, a large increase in remanence on cooling in RTSIRM, a magnetically hard, low-unblocking temperature phase in the modified Lowrie tests, and distinct high-coercivity peaks observed in FORC analysis. As this behavior is effectively identical to that described previously for strongly baked sediment and porcellanite samples, we will not detail it further here.

Minor components of three other magnetic minerals were also identified in paralavas: hematite, intermediate titanohematite, and native Fe. Evidence for hematite comes from the HT hysteresis experiment, which displayed a sharp increase in B_c at temperatures $> 600^\circ\text{C}$ (Figure S3H). Additionally, some paralava samples in the field had red oxidized surficial alteration rinds that were not pervasive in drill cores. This red color is suggestive of oxidation to hematite. Evidence for intermediate titanohematite comes from the modified Lowrie experiment. Each of the two specimens that were included in the modified Lowrie experiment contained a low T_{ub} phase that displayed an initial drop in remanence that is then completely regained, suggestive of self-reversed intermediate titanohematite (CNF8-2C, Figure 9d; CNF5-6c; Figure S6D). In one specimen, remanence is regained by AF fields of ~ 30 mT (CNF5-6c; Figure S6D). In the other, the remanence held by the low-blocking temperature phase is entirely negative, and is completely removed by 170 mT, suggesting that this remanence is entirely held by intermediate titanohematite (CNF8-2C, Figure 9d). $k(T)$ experiments additionally show evidence of this low-unblocking temperature phase, with one specimen (CNFP3-12) showing additional Curie points at 223°C and 413°C (Figure 5f). Native iron is also possibly present in this sample (CNFP3-12), as evidenced by $k(T)$ data (Figure 5f) showing a phase with remaining susceptibility ~ 700 – 720°C , the peak temperature for these experiments.

The laboratory induced ARM value for the one measured paralava is 2×10^{-4} Am²/kg, generally larger than unbaked sediments, but not as strong as baked sediments.

4.2. Color/Oxidation State

In general, there is no statistically robust covariance between color and hysteresis data (Figures S2A–S2D). The HCSLT component occurs in orange and red samples, but is possibly more prevalent in orange samples (Figure S2A). This behavior suggests that the HCSLT phase forms in oxidizing conditions.

4.3. Profiles

In our two measured profiles, we performed ARM demagnetization, frequency dependence of susceptibility, and HT susceptibility experiments to assess whether magnetic properties vary with distance from the coal seam fire. In general, we observe no discernable trend in magnetic properties with distance above the coal seam, but there are large differences between the unbaked sediment immediately below the remnant coal seam and the clinker material above. This difference is diminished in more weakly baked clinker deposits.

Profile CNFP3 is the more strongly baked profile in this study and examines a section from 2 m below to 8 m above a burnt coal seam. At the stratigraphically lowest point, unbaked sediment transitions to coal ash, then clinker breccia, followed by porcellanite mixed with layers of paralava, and finally to a baked sandstone which forms the caprock for a local butte. In general, this profile highlights the clear difference

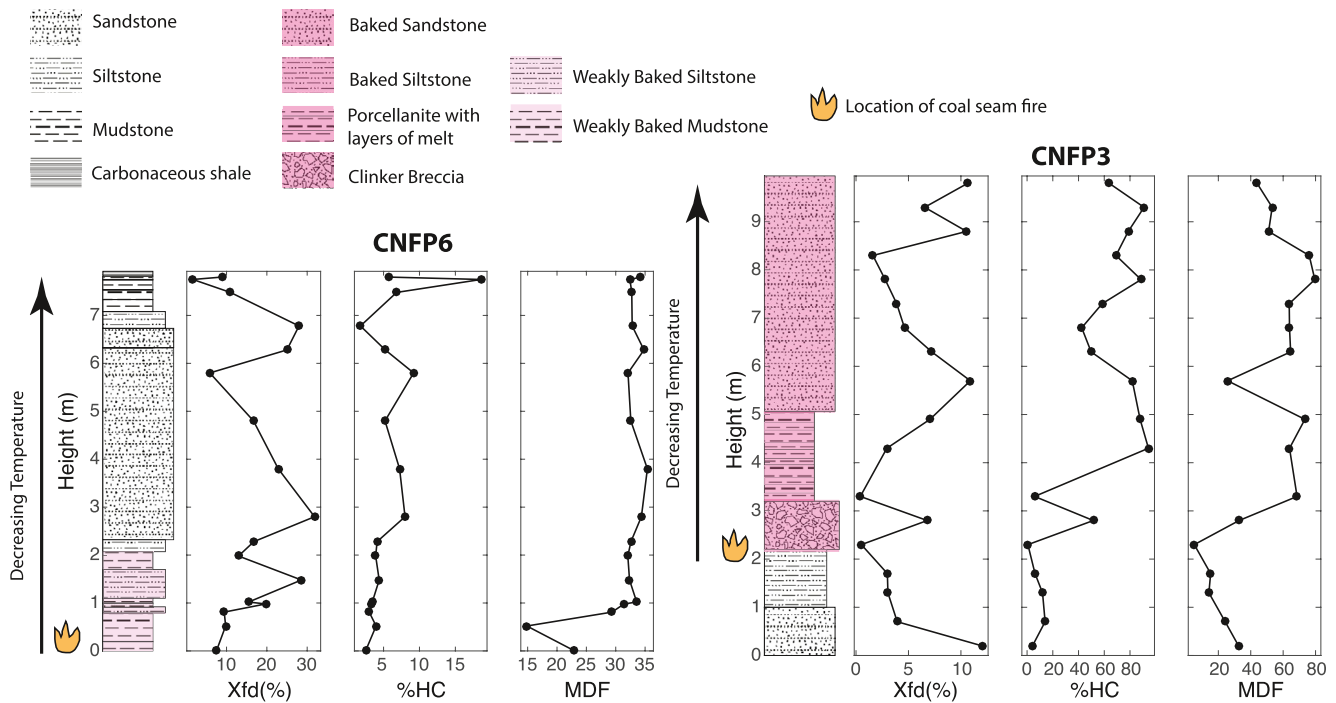


Figure 11. Stratigraphy and magnetic data for the two profile sections, where %HC is percent high-coercivity, MDF is median destructive field (both determined from anhysteretic remanent magnetization demagnetization experiments), and χ_{fd} is frequency dependence of susceptibility.

in magnetic behavior between the unbaked material immediately below the coal seam, and the clinker products above (Figure 11) but we do not find observable differences in magnetic properties as a function of distance from the coal seam that are not already encompassed by lithology. The unbaked material in the 2 m below the coal seam shows very little sign of magnetic alteration from the coal fire. All but two unbaked samples alter during heating in $k(T)$ experiments (CNFP3-17 and CNFP6-14; Figures S4F and S4J), all samples have very low %HC ~4%–14% and relatively low χ_{fd} values, ranging from 2% to 4% (Figures 11, S2E and S2F). Immediately, at the base of the clinker deposits above the coal ash layer, magnetic properties change to those diagnostic of strongly baked clinker lithologies. Although there is variation in %HC, χ_{fd} , and MDFs (Figures 11, S2E, S2F and S2H) throughout the profile, none of these variations are a function of distance from the coal seam. Instead, the largest difference between samples in the section is dependent upon lithology, where paralaava and ash samples have the lowest %HC values, suggesting that the HCSLT phase is not abundant in these materials. Note, that although the %HC values for the unbaked samples are minimum estimates, we did not find evidence for high-coercivity phases in high- T hysteresis experiments. As such, we believe that the high-coercivity phases identified in the strongly baked materials were created by baking. There is also no trend with laboratory-induced ARM and distance from the coal seam beyond a large increase in ARM values as one transitions from unbaked to strongly baked material (Figure S10; Table S1).

Profile CNFP6 is a more weakly baked clinker and examines an 8 m section that grades into unbaked sediment at the top. In general, there is very little difference between the weakly baked and unbaked sediment in this profile (Figure 11). One observable difference between the weakly baked and unbaked specimens is that the laboratory-induced ARM is slightly higher for the weakly baked specimens, and progressively decreases to a reproducible baseline level as one moves away from the burnt coal seam (Figure S10). The lowest reproducible ARM values are not found until many meters away from the base of the burnt coal. It is important to note that the %HC values for this profile are representative of the laboratory DRM and as such it is possible that more variation in NRM may occur between weakly baked and unbaked materials than is reported here.

These profiles highlight a few key findings: (a) to produce the magnetic mineral changes observed between unbaked sediment and strongly baked clinker products, a coal seam fire must burn longer and/or hotter than that which produced profile CNFP6, (b) the HCSLT phase does not appear to form in weakly baked sediments, but occurs throughout our strongly baked profile, (c) unbaked and strongly baked materials show significant differences in magnetic properties transitioning at the base of the burnt coal seam, and (d) magnetic properties do not vary dramatically between the weakly baked and unbaked sediment, though the variation in ARM intensity in our profile suggests that even weak coal fires are affecting the magnetic mineralogy of surrounding sediments in a perceptible manner.

4.4. Locality

Overall, there is no observable difference between magnetic properties as a function of locality or coal zone (Figure S11). What this suggests is that the fundamental processes that control the observed magnetic mineralogy of clinker deposits in fluvial sediments is the formation of new magnetic materials during baking, and not primary lithology nor primary magnetic materials, at least on a regional scale.

5. Discussion

5.1. Mineralogy of the HCSLT Phase

We interpret the HCSLT phase identified in the baked clinker samples as $\epsilon\text{-Fe}_2\text{O}_3$ (“Luogufengite”). $\epsilon\text{-Fe}_2\text{O}_3$ is a rare metastable polymorph of iron (III) oxide that lies between stable end-members $\gamma\text{-Fe}_2\text{O}_3$ (maghemite) and $\alpha\text{-Fe}_2\text{O}_3$ (hematite). Despite having many similarities with its stable end-members, the magnetic behavior of $\epsilon\text{-Fe}_2\text{O}_3$ is distinctly different. Because of the material’s relatively disordered structure and its large magnetocrystalline anisotropy, $\epsilon\text{-Fe}_2\text{O}_3$ possesses a large, 2 T, coercive field at room temperature, similar in scale to hematite (MacHala et al., 2011). Unlike hematite, $\epsilon\text{-Fe}_2\text{O}_3$ is collinear ferrimagnetic with a low Curie temperature of $\sim 495\text{K}$ (222°C) and a significantly higher saturation magnetization of $15\text{--}25\text{ Am}^2\text{ kg}^{-1}$ (Xu et al., 2017). A low- T transition has also been reported at $\sim 110\text{K}$ and is marked by a decrease in coercive field strength on cooling (MacHala et al., 2011; Tucek et al., 2010).

These particular magnetic properties (low Curie temperature, high-coercivity, and high magnetization) are consistent with the HCSLT phase identified in our clinker samples in addition to the HCSLT phase identified in a range of baked archeological materials (McIntosh et al., 2007, 2011). Some minor variations between the HCSLT phase identified in clinkers and archeological materials relative to synthetic $\epsilon\text{-Fe}_2\text{O}_3$ have been observed, including lower unblocking temperatures ($\sim 175\text{--}225^\circ\text{C}$ and $170\text{--}190^\circ\text{C}$, respectively) and additionally, both clinkers and archeological materials do not show evidence of the low- T transition. Despite this, using confocal Raman spectroscopy, López-Sánchez et al. (2017, 2020) identified the HCSLT phase in archeological artifacts as $\epsilon\text{-Fe}_2\text{O}_3$. In these studies, the authors argued that the slightly lower observed Curie points and lack of low- T transition is likely due to cation substitution in the crystal lattice of $\epsilon\text{-Fe}_2\text{O}_3$ (López-Sánchez et al., 2017). However, few magnetic experiments on cation substituted $\epsilon\text{-Fe}_2\text{O}_3$ exist, and as such some authors, for example, Kosterov et al. (2021), are more hesitant in definitively assigning the HCSLT phase in archeological samples to $\epsilon\text{-Fe}_2\text{O}_3$, particularly for samples where the Curie points for the observed HCSLT phase are low ($120\text{--}140^\circ\text{C}$). Based on the similarities between the magnetic properties of our HCSLT phase with that found in archeological materials, in addition to the similar formation mechanisms (i.e., the heating of clays to high- T in an oxidizing environment), we conclude that the HCSLT phase in clinker deposits is likely the same as that found in archeological materials and that, given the available data, it is most likely a cation-substituted variant of $\epsilon\text{-Fe}_2\text{O}_3$.

Although $\epsilon\text{-Fe}_2\text{O}_3$ is purportedly rare in nature, other naturally occurring $\epsilon\text{-Fe}_2\text{O}_3$ has been identified in vesicles of late Pleistocene basaltic scoria, in almandine garnets, and in baked nontronite (Barcova et al., 2001; Kelm & Mader, 2005; Petersen et al., 1987; Tucek et al., 2010; Xu et al., 2017). The discovery of $\epsilon\text{-Fe}_2\text{O}_3$ in clinker deposits greatly expands the occurrence of the mineral in nature and indicates that it may be a more abundant natural carrier of magnetic remanence than previously believed.

5.2. Acquisition of Magnetization in Clinkers

Comparing the rock magnetic data from unbaked, weakly baked, strongly baked (including porcellanite), and paralava material in clinker deposits, we conclude that clinker deposits acquire magnetization in two primary ways: (a) thermal remagnetization, and (b) the formation and growth of new magnetic minerals. Our results are largely consistent with previous studies, but we can provide important new details to the process of clinker magnetic acquisition. In unbaked materials, the primary magnetic mineralogy is intermediate titanomagnetite (or titanohematite), marked by low Curie temperatures ($<400^{\circ}\text{C}$) and hysteresis behavior consistent with a soft ferrimagnetic mineral. Upon ignition of the coal seam, close to the fire, new magnetic particles form (magnetite, possibly from clay alteration, and hematite, possibly from goethite dehydration) and temperatures are hot enough to reset the magnetic recording. This is evidenced by the appearance of magnetite in weakly baked samples, their elevated ARMs and thermal stability compared to unbaked material, and their red color. Many meters above the coal seam, where there is no apparent oxidation of the sediments, the coal fire still nucleated and grew sufficient magnetite to produce elevated ARMs in the weakly baked profile. Although temperatures close to the coal fire are likely hot enough to completely reset the primary magnetic recording (at least $>400^{\circ}\text{C}$, based on laboratory clay alteration and goethite dehydration experiments; this study; Özdemir & Dunlop, 2000; Sprain et al., 2016), it is difficult to assess whether the magnetic recording held by the newly formed magnetite and hematite in weakly baked samples is a TRM or a TCRM. Further, if it is a TRM, at some unknown distance from the coal seam, it would be expected to transition to a TCRM or pTRM.

If the coal fire persists and continues to burn for longer periods of time, the magnetic mineral assemblage changes even more, and a new magnetic phase forms in oxidizing regions ($\epsilon\text{-Fe}_2\text{O}_3$). It is unclear what the temperature or duration of heating is needed to form $\epsilon\text{-Fe}_2\text{O}_3$, but what is clear is that the mineral is abundant in strongly baked clinker lithologies (porcellanite and strongly baked sediments) and we did not find evidence of it in weakly baked clinker lithologies (albeit more experiments are needed to confirm this), suggesting that its formation is a function of temperature and/or time. In laboratory settings, when embedded in a silica matrix, typical temperature ranges for the formation and stability of Fe_2O_3 polymorphs are $\gamma\text{-Fe}_2\text{O}_3$ ($<950^{\circ}\text{C}$), $\epsilon\text{-Fe}_2\text{O}_3$ ($950\text{--}1300^{\circ}\text{C}$), and $\alpha\text{-Fe}_2\text{O}_3$ (above 1300°C) (MacHala et al., 2011; Ohkoshi et al., 2015). However, it has been shown that these temperatures can vary depending on particle size, dopants, and degree of agglomeration (MacHala et al., 2011). For example, $\epsilon\text{-Fe}_2\text{O}_3$ has been observed to form via the heating of nontronite (an Fe-rich smectitic clay that also occurs on the Martian surface) to 900°C with annealing times over 3 h (Moskowitz & Hargraves, 1982, 1984). However, in replica archeological kilns, the HCSLT phase thought to be cation substituted $\epsilon\text{-Fe}_2\text{O}_3$ has been shown to form at temperatures as low as 750°C , with little to no annealing time (Calvo-Rathert et al., 2019). Additionally, due to the material's low surface energy, the grain size of pure $\epsilon\text{-Fe}_2\text{O}_3$ is limited to <30 nm (Gich et al., 2007), with inversion to hematite occurring as growth continues beyond this threshold. However, larger grain sizes of $\epsilon\text{-Fe}_2\text{O}_3$ have been synthesized in the laboratory (100–200 nm) (Tucek et al., 2010) and micrometer-size $\epsilon\text{-Fe}_2\text{O}_3$ crystals have been identified in archeological materials (Dejoie et al., 2014; López-Sánchez et al., 2017). This difference in size (in addition to small shifts in the magnetic properties observed between natural and laboratory material) has been suggested to be due to cation substitution (López-Sánchez et al., 2017). Whether cation substitution leads to an increase in stability of $\epsilon\text{-Fe}_2\text{O}_3$ and promotes larger particle size, and whether this substitution changes the parameters (such as temperature) that control the γ , ϵ , and α transitions, needs further study.

Although it is unclear at what temperature $\epsilon\text{-Fe}_2\text{O}_3$ forms in nature, available evidence suggests that it is likely at high temperatures, $>600^{\circ}\text{C}$. $\epsilon\text{-Fe}_2\text{O}_3$ is abundant in strongly baked sediments and porcellanite and is found as much as 8 m above the burnt coal seam. If the available information on formation temperature of this phase is accurate for clinker deposits, it suggests that coal seam fires were able to maintain high temperatures ($>600^{\circ}\text{C}$) over large distances (>8 m) from the coal seam fire. This estimate is generally consistent with thermal models that suggest that burning coal seams can maintain high temperatures many meters away from the burn front (Wessling et al., 2008). The results are also consistent with geochemical analysis showing the presence of other high- T phases, like mullite, cordierite, and cristobalite, in clinker materials (Cosca et al., 1989; Estrada et al., 2009; Novikov et al., 2008; Novikova et al., 2016; Sokol et al., 2014). Due to the low Curie temperature of $\epsilon\text{-Fe}_2\text{O}_3$, this phase most likely holds a TRM. If magnetite had already formed,

which is probable based on evidence from our weakly baked samples, or was forming during the formation of ϵ -Fe₂O₃, then it also most likely holds a TRM.

In vents or regions within the coal seam where temperatures exceeded 1000°C, sediments are further transformed and they begin to melt and recrystallize to form paralavas. Whether the magnetite phase in paralavas was inherited from pre-melted material or whether it crystallized out of the melt during cooling, it most likely holds a TRM so long as it has not undergone low-*T* oxidation at a later time period.

Although our conclusions are drawn from a limited study area, we believe they are applicable to other clinker deposits around the world. Our results show that the fundamental processes that control the observed magnetic mineralogy of clinker deposits is the formation of new magnetic materials during baking, and is not dependent on primary lithology (limited to fluvial origin) nor primary magnetic materials. As such, it follows that clinkers derived from fluvial protoliths found in other sedimentary basins should have similar magnetic behavior to those studied here.

5.3. Implications for Paleodirectional and Paleointensity Studies

The rock magnetic data presented here confirm that clinkers have the capacity to be reliable recorders of the paleomagnetic field for both direction and intensity. Within baked profiles, two dominant mineralogies emerged; magnetite and ϵ -Fe₂O₃. In the paralavas, the dominant mineralogy is magnetite. As shown in the previous section, temperatures achieved during clinker formation should have been sufficiently high to overwrite the original DRM with a TRM. Furthermore, the occurrence of ϵ -Fe₂O₃ in strongly baked deposits suggests that clinkers formed at extremely high-*T*, possibly above the Curie point of either mineral. Based on the coercivities of the magnetite and ϵ -Fe₂O₃, we can assume that a TRM held by either mineral in clinker deposits should be maintained over geologic timescales. Further, paleomagnetic experiments on archeological materials that contain both magnetite and ϵ -Fe₂O₃ components show that the mineralogies record similar directions and intensities (López-Sánchez et al., 2017; McIntosh et al., 2007, 2011). These data passed all standard paleointensity reliability criteria and produced robust results (McIntosh et al., 2011). Additionally, strongly baked sediments, porcellanites, and paralavas are all thermally stable upon reheating, which is a necessary requirement for thermally based paleointensity methods. In summary, both the ϵ -Fe₂O₃ and magnetite phases should record primary TRMs from the time of clinker formation that are held by grain sizes whose magnetizations are stable on geologic timescales and do not alter during laboratory heating. Thus, strongly baked clinker material should be ideal for paleodirectional and paleointensity studies, and we encourage sampling closer to the coal seam to have a higher probability of samples holding a TRM.

This conclusion is confirmed by our preliminary paleodirectional and paleointensity experiments, an example of which for strongly baked mudstone samples from clinker Undated-4 (CNF10) is shown in Figure 12. Thermal demagnetization results show stable directions that trend toward the origin, which are consistent between three separately oriented samples. The paleointensity results show near ideal straight-line behavior on Arai plots, no significant alteration, and consistency between the estimated B_{anc} for all three samples.

Despite their seemingly ideal magnetic mineralogy, there are still some complexities that will need to be assessed in future paleodirectional and paleointensity studies to ascertain whether intensity and directional measurements from clinkers are reliable. These include timing of slumping, cooling rate, anisotropy, and nonlinear remanence. Experiments assessing these are ongoing.

6. Conclusions

Extensive rock magnetic analysis on Quaternary clinker deposits from the Custer National Forest, SE Montana demonstrate that strongly baked clinker deposits show all of the hallmarks of reliable recorders of magnetic remanence. Results show that strongly baked clinker materials (porcellanite and strongly baked sediment) contain two main magnetic carriers, magnetite and ϵ -Fe₂O₃, with minor contributions from hematite and intermediate titanohematite. Paralavas are dominated by one main magnetic carrier, which is magnetite. Magnetic properties do not vary systematically with distance from the coal seam, by primary lithology, or by locality. Oxidation state does appear to have a minor effect on enhancing the ϵ -Fe₂O₃ component, but the primary control on magnetic mineralogy is clinker lithology. Strongly baked clinkers produce

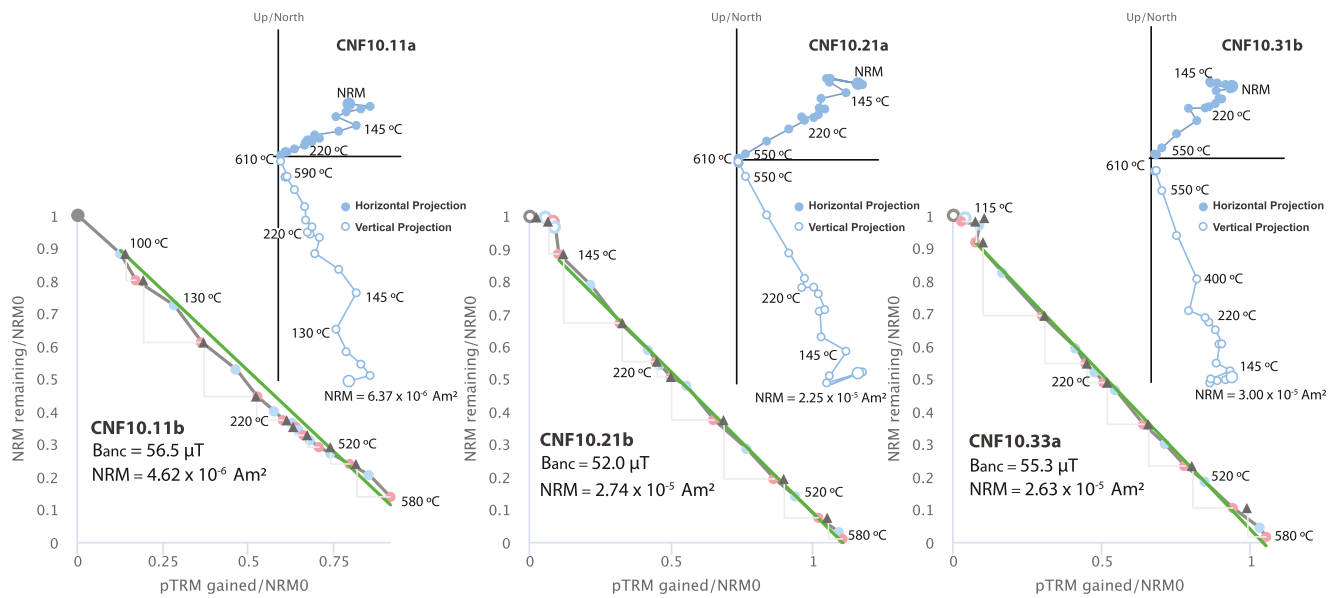


Figure 12. Characteristic results of thermal demagnetization experiments and Thellier style (Thellier & Thellier, 1959) paleointensity using the IZZI method (Tauxe & Staudigel, 2004; Yu et al., 2004) experiments displayed on Zijderveld (inset) and Arai plots for Undated-4 clinker, CNF10. Blue (red) circles indicate zero-field/in-field (in-field/zero-field) steps “ZI” (“IZ”). Triangles mark partial thermoremanent magnetization (pTRM) checks. Closed and open circles in the Zijderveld plots are horizontal and vertical projections, respectively, of the natural remanent magnetizations (NRMs) in specimen coordinates. Estimates of the ancient field (Banc) are shown for each specimen. Paleodirectional data were analyzed using [Paleomagnetism.org](https://paleomagnetism.org) (Koymans et al., 2016) and paleointensity data were analyzed using [Paleointensity.org](https://paleointensity.org) (Beguin et al., 2020).

Acknowledgments

The authors thank the Institute for Rock Magnetism (IRM), the UK National Environmental Research Council, and the University of Liverpool for support of this work. Sample analysis was funded by an IRM visiting fellowship awarded to the first author and the UMN Undergraduate Research Opportunity Program awarded to the third author. Field work was funded by the University of Liverpool’s Early Career and Returners fund awarded to Courtney J. Sprain. Courtney J. Sprain was additionally funded by the Natural Environment Research Council (NERC standard grant, NE/P00170X/1) and Richard K. Bono was supported by the Leverhulme Trust (Research Leadership Award, RL-2016-080; Early Career Fellowship, ECF-2020-617). The authors further thank Yael Engbers and Daniele Thallner at the University of Liverpool for help with field work. The authors also thank Andrew Biggin for his support on this project. The authors would also like to thank the entire IRM staff for their overwhelming support and kindness and especially Bruce Moskowitz who pointed us in the direction of ϵ -Fe₂O₃. The authors additionally thank Jérôme Gattacceca and Lisa Tauxe for their constructive reviews.

magnetic mineral assemblages that are thermally stable and cool from temperatures higher than the Curie point of magnetite, even as far away as 8 m from the coal seam. This suggests that samples collected from close to the coal seam fire will likely record a TRM. Additionally, coercivity analysis and preliminary paleointensity results indicates that the magnetic minerals in clinkers are amenable to high-quality paleointensity study. Overall, our study suggests that clinkers should be reliable full vector paleomagnetic recorders. Future experiments assessing cooling rate, anisotropy, the timing of slumping, and the formation of ϵ -Fe₂O₃ in nature are needed to further assess the reliability of clinker magnetic remanence.

Conflict of Interest

The authors declare no conflicts of interest relevant to this study.

Data Availability Statement

The data presented in the paper can be found in the MagIC database (Sprain et al., 2021; doi:10.7288/V4/MAGIC/19216) and in Supporting Information S1.

References

- Barcova, K., Mashlan, M., Zboril, R., Martinec, P., & Kula, P. (2001). Thermal decomposition of almandine garnet: Mössbauer study. *Czechoslovak Journal of Physics*, 51(7), 749–754. <https://doi.org/10.1023/a:1017618420189>
- Beguin, A., Paterson, G. A., Biggin, A. J., & de Groot, L. V. (2020). Paleointensity.org: An online, open source, application for the interpretation of paleointensity data. *Geochemistry, Geophysics, Geosystems*, 21(5), e2019GC008791. <https://doi.org/10.1029/2019gc008791>
- Belt, E. S., Hartman, J. H., Diemer, J. A., Kroeger, T. J., Tibert, N. E., & Curran, H. A. (2004). Unconformities and age relationships, Tongue River and older members of the Fort Union Formation (Paleocene), western Williston Basin, U.S.A. *Rocky Mountain Geology*, 39(2), 113–140. <https://doi.org/10.2113/39.2.113>
- Biggin, A. J., Piispa, E. J., Pesonen, L. J., Holme, R., Paterson, G. A., Veikkolainen, T., & Tauxe, L. (2015). Palaeomagnetic field intensity variations suggest Mesoproterozoic inner-core nucleation. *Nature*, 526(7572), 245–248. <https://doi.org/10.1038/nature15523>
- Bucha, V., Horáček, J., & Rybář, J. (1968). The intensity of the geomagnetic field in the Quaternary. *Studia Geophysica et Geodaetica*, 12(1), 56–62. <https://doi.org/10.1007/bf02585084>

- Calvo-Rathert, M., Contreras, J. M., Carrancho, Á., Camps, P., Goguitaichvili, A., & Hill, M. J. (2019). Reproducibility of archaeointensity determinations with a multimethod approach on archaeological material reproductions. *Geophysical Journal International*, 218(3), 1719–1738. <https://doi.org/10.1093/gji/ggz246>
- Church, N., Feinberg, J. M., & Harrison, R. (2011). Low-temperature domain wall pinning in titanomagnetite: Quantitative modeling of multidomain first-order reversal curve diagrams and AC susceptibility. *Geochemistry, Geophysics, Geosystems*, 12(7). <https://doi.org/10.1029/2011gc003538>
- Cisowski, S. M., & Fuller, M. (1987). Generation of magnetic anomalies by combustion metamorphism of sedimentary rock, and its significance to hydrocarbon exploration. *Bulletin of the Geological Society of America*, 99(1), 21–29. [https://doi.org/10.1130/0016-7606\(1987\)99<21:TGOMAB>2.0.CO;2](https://doi.org/10.1130/0016-7606(1987)99<21:TGOMAB>2.0.CO;2)
- Coates, D. A., & Heffern, E. L. (1999). *Origin and geomorphology of clinker in the Powder River Basin, Wyoming and Montana*.
- Coates, D. A., & Heffern, E. L. (2000). Origin and geomorphology of clinker in the Powder River Basin, Wyoming and Montana. In R. Miller (Ed.), *Coalbed methane and Tertiary geology of the Powder River Basin, Wyoming geological association 50th annual field conference guidebook* (pp. 211–229). Casper.
- Constable, C., Korte, M., & Panovska, S. (2016). Persistent high paleosecular variation activity in southern hemisphere for at least 10000 years. *Earth and Planetary Science Letters*, 453, 78–86. <https://doi.org/10.1016/j.epsl.2016.08.015>
- Cosca, M., Essene, E. J., Geissman, J. W., Simmons, W. B., & Coates, D. A. (1989). Pyrometamorphic rocks associated with naturally burned coal beds, Powder River Basin, Wyoming. *American Mineralogist*, 74, 85–100.
- Day, R., Fuller, M., & Schmidt, V. A. (1977). Hysteresis properties of titanomagnetites: Grain-size and compositional dependence. *Physics of the Earth and Planetary Interiors*, 13(4), 260–267. [https://doi.org/10.1016/0031-9201\(77\)90108-x](https://doi.org/10.1016/0031-9201(77)90108-x)
- de Boer, C. B., Dekkers, M. J., & van Hoof, T. A. M. (2001). Rock-magnetic properties of TRM carrying baked and molten rocks straddling burnt coal seams. *Physics of the Earth and Planetary Interiors*, 126(1–2), 93–108. [https://doi.org/10.1016/S0031-9201\(01\)00246-1](https://doi.org/10.1016/S0031-9201(01)00246-1)
- Dejoie, C., Sciau, P., Li, W., Noé, L., Mehta, A., Chen, K., et al. (2014). Learning from the past: Rare ϵ -Fe₂O₃ in the ancient black-glazed Jian (Tenmoku) wares. *Scientific Reports*, 4, 1–9. <https://doi.org/10.1038/srep04941>
- Dekkers, M. J. (1989). Magnetic properties of natural goethite—II. TRM behaviour during thermal and alternating field demagnetization and low-temperature treatment. *Geophysical Journal International*, 97(2), 341–355. <https://doi.org/10.1111/j.1365-246x.1989.tb00505.x>
- Dunlop, D. J., & Özdemir, Ö. (2001). *Rock magnetism: Fundamentals and frontiers*. Cambridge University Press.
- Egli, R. (2013). VARIFORC: An optimized protocol for calculating non-regular first-order reversal curve (FORC) diagrams. *Global and Planetary Change*, 110, 302–320. <https://doi.org/10.1016/j.gloplacha.2013.08.003>
- Estrada, S., Piepjohn, K., Frey, M. J., Reinhardt, L., Andruleit, H., & Von Gosen, W. (2009). Pliocene coal-seam fires on southern Ellesmere Island, Canadian Arctic. *Neues Jahrbuch Fur Geologie Und Palaontologie—Abhandlungen*, 251(1), 33–52. <https://doi.org/10.1127/0077-7749/2009/0251-0033>
- Fabian, K. (2003). Some additional parameters to estimate domain state from isothermal magnetization measurements. *Earth and Planetary Science Letters*, 213(3–4), 337–345. [https://doi.org/10.1016/s0012-821x\(03\)00329-7](https://doi.org/10.1016/s0012-821x(03)00329-7)
- Fabian, K., Miyajima, N., Robinson, P., McEnroe, S. A., Ballaran, T. B., & Burton, B. P. (2011). Chemical and magnetic properties of rapidly cooled metastable ferri-ilmenite solid solutions: Implications for magnetic self-reversal and exchange bias—I. Fe-Ti order transition in quenched synthetic ilmenite 61. *Geophysical Journal International*, 186(3), 997–1014. <https://doi.org/10.1111/j.1365-246x.2011.05109.x>
- Flores, R., & Bader, L. (1999). *Fort Union coal in the Powder River Basin, Wyoming and Montana: A synthesis* (p. 1625). US Geological Survey Professional Paper.
- France, D. E., & Oldfield, F. (2000). Identifying goethite and hematite from rock magnetic measurements of soils and sediments. *Journal of Geophysical Research*, 105(B2), 2781–2795. <https://doi.org/10.1029/1999jb900304>
- Gich, M., Roig, A., Taboada, E., Molins, E., Bonafos, C., & Snoeck, E. (2007). Stabilization of metastable phases in spatially restricted fields: The case of the Fe₂O₃ polymorphs. *Faraday Discussions*, 136, 345–354. <https://doi.org/10.1039/b616097b>
- Grapes, R. (2010). *Pyrometamorphism*. Springer Science & Business Media.
- Harrison, R. J., & Feinberg, J. M. (2008). FORCinel: An improved algorithm for calculating first-order reversal curve distributions using locally weighted regression smoothing. *Geochemistry, Geophysics, Geosystems*, 9(5). <https://doi.org/10.1029/2008gc001987>
- Heffern, E. L., & Coates, D. A. (1997). *Clinker-its occurrence, uses, and effects on coal mining in the Powder River Basin*. Proceedings of the 32nd annual forum on the geology of industrial minerals: Wyoming State Geological Survey Public Information Circular (Vol. 38, pp. 151–165).
- Heffern, E. L., & Coates, D. A. (2004). Geologic history of natural coal-bed fires, Powder River Basin, USA. *International Journal of Coal Geology*, 59(1–2), 25–47. <https://doi.org/10.1016/j.coal.2003.07.002>
- Heffern, E. L., Reiners, P. W., Naeser, C. W., & Coates, D. A. (2007). Geochronology of clinker and implications for evolution of the Powder River Basin landscape, Wyoming and Montana. In *Geology of coal fires: Case studies from around the world* (Vol. XVIII, pp. 155–175). [https://doi.org/10.1130/2007.4118\(10\)](https://doi.org/10.1130/2007.4118(10))
- Heffern, E. L., Reiners, P. W., & Riihimaki, C. A. (2013). Clinker distribution and age in the Powder River structural basin. *Montana Bureau of Mines and Geology Geologic Map*, 64(1), 339–849.
- Hooper, R. L. (1987). Factors affecting the magnetic susceptibility of baked rocks above a burned coal seam. *International Journal of Coal Geology*, 9(2), 157–169. [https://doi.org/10.1016/0166-5162\(87\)90043-7](https://doi.org/10.1016/0166-5162(87)90043-7)
- Jones, A. H., Geissman, J. W., & Coates, D. A. (1984). Clinker Deposits, Powder River Basin, Wyoming and Montana: A new source of high-fidelity paleomagnetic data for the Quaternary. *Geophysical Research Letters*, 11, 1231–1234. <https://doi.org/10.1029/gl011i012p01231>
- Kelm, K., & Mader, W. (2005). Synthesis and structural analysis of ϵ -Fe₂O₃. *Zeitschrift für Anorganische und Allgemeine Chemie*, 631(12), 2383–2389. <https://doi.org/10.1002/zaac.200500283>
- Khesin, B., Feinstein, S., Vapnik, Y., Itkis, S., & Leonhardt, R. (2005). Magnetic study of metamorphosed sedimentary rocks of the Hatrum formation, Israel. *Geophysical Journal International*, 162(1), 49–63. <https://doi.org/10.1111/j.1365-246X.2005.02630.x>
- Korte, M., & Constable, C. G. (2003). Continuous global geomagnetic field models for the past 3000 years. *Physics of the Earth and Planetary Interiors*, 140(1–3), 73–89. <https://doi.org/10.1016/j.pepi.2003.07.013>
- Korte, M., & Constable, C. G. (2005). The geomagnetic dipole moment over the last 7000 years—New results from a global model. *Earth and Planetary Science Letters*, 236(1–2), 348–358. <https://doi.org/10.1016/j.epsl.2004.12.031>
- Korte, M., & Constable, C. G. (2011). Improving geomagnetic field reconstructions for 0–3 ka. *Physics of the Earth and Planetary Interiors*, 188(3–4), 247–259. <https://doi.org/10.1016/j.pepi.2011.06.017>
- Korte, M., Constable, C. G., Donadini, F., & Holme, R. (2011). Reconstructing the Holocene geomagnetic field. *Earth and Planetary Science Letters*, 312(3–4), 497–505. <https://doi.org/10.1016/j.epsl.2011.10.031>

- Kosterov, A., Kovacheva, M., Kostadinova-Avramova, M., Minaev, P., Salnaia, N., Surovitskii, L., et al. (2021). High-coercivity magnetic minerals in archaeological baked clay and bricks. *Geophysical Journal International*, 224(2), 1256–1271.
- Koymans, M. R., Langereis, C. G., Pastor-Galán, D., & van Hinsbergen, D. J. J. (2016). Paleomagnetism.org: An online multi-platform open source environment for paleomagnetic data analysis. *Computers & Geosciences*, 93, 127–137. <https://doi.org/10.1016/j.cageo.2016.05.007>
- Krs, M. (1968). Geomagnetic field intensity during the Plio-Pleistocene derived from the thermo-remance of porcellanites and palaeo-slugs (Czechoslovakia). *Pure and Applied Geophysics PAGEOPH*, 69(1), 158–167. <https://doi.org/10.1007/BF00874913>
- Krsová, M., Krs, M., Pruner, P., Chvojka, R., & Kropáček, V. (1989). Palaeointensity of the geomagnetic field during upper cainozoic derived from palaeo-slugs and porcellanites in north Bohemia. *Studia Geophysica et Geodaetica*, 33(4), 338–361. <https://doi.org/10.1007/bf01637689>
- Kuenzer, C., & Stracher, G. B. (2012). Geomorphology of coal seam fires. *Geomorphology*, 138(1), 209–222. <https://doi.org/10.1016/j.geomorph.2011.09.004>
- Lammer, H., Bredehöft, J. H., Coustenis, A., Khodachenko, M. L., Kaltenecker, L., Grasset, O., et al. (2009). What makes a planet habitable? *Astronomy and Astrophysics Review*, 17(2), 181–249. <https://doi.org/10.1007/s00159-009-0019-z>
- Lifton, N., Sato, T., & Dunai, T. J. (2014). Scaling in situ cosmogenic nuclide production rates using analytical approximations to atmospheric cosmic-ray fluxes. *Earth and Planetary Science Letters*, 386, 149–160. <https://doi.org/10.1016/j.epsl.2013.10.052>
- Lindqvist, J. K., Hatherton, T., & Mumme, T. C. (1985). Magnetic anomalies resulting from baked sediments over burnt coal seams in southern New Zealand. *New Zealand Journal of Geology and Geophysics*, 28(3), 405–412. <https://doi.org/10.1080/00288306.1985.10421195>
- López-Sánchez, J., McIntosh, G., Osete, M. L., Del Campo, A., Villalain, J. J., Pérez, L., et al. (2017). Epsilon iron oxide: Origin of the high coercivity stable low Curie temperature magnetic phase found in heated archeological materials. *Geochemistry, Geophysics, Geosystems*, 18(7), 2646–2656.
- López-Sánchez, J., Palencia-Ortas, A., del Campo, A., McIntosh, G., Kovacheva, M., Martín-Hernández, F., et al. (2020). Further progress in the study of epsilon iron oxide in archaeological baked clays. *Physics of the Earth and Planetary Interiors*, 307, 106554. <https://doi.org/10.1016/j.pepi.2020.106554>
- Lowrie, W. (1990). Identification of ferromagnetic minerals in a rock by coercivity and unblocking temperature properties. *Geophysical Research Letters*, 17(2), 159–162. <https://doi.org/10.1029/gl017i002p00159>
- Lowrie, W., & Heller, F. (1982). Magnetic properties of marine limestones. *Reviews of Geophysics*, 20(2), 171–192. <https://doi.org/10.1029/rg020i002p00171>
- Luppens, J. A., Scott, D. C., Haacke, J., Osmonson, L. M., & Pierce, P. E. (2015). *Coal geology and assessment of coal resources and reserves in the Powder River Basin, Wyoming and Montana*. US Geological Survey. <https://doi.org/10.3133/pp1809>
- MacHala, L., Tuček, J., & Zboril, R. (2011). Polymorphous transformations of nanometric iron (III) oxide: A review. *Chemistry of Materials*, 23(14), 3255–3272. <https://doi.org/10.1021/cm200397g>
- McIntosh, G., Kovacheva, M., Catanzariti, G., Donadini, F., & Lopez, M. L. O. (2011). High coercivity remanence in baked clay materials used in archeomagnetism. *Geochemistry, Geophysics, Geosystems*, 12(2). <https://doi.org/10.1029/2010GC003310>
- McIntosh, G., Kovacheva, M., Catanzariti, G., Osete, M. L., & Casas, L. (2007). Widespread occurrence of a novel high coercivity, thermally stable, low unblocking temperature magnetic phase in heated archeological material. *Geophysical Research Letters*, 34(21), 1–5. <https://doi.org/10.1029/2007GL031168>
- Moskowitz, B. M., & Hargraves, R. B. (1982). Magnetic changes accompanying the thermal decomposition of nontronite (in air) and its relevance to Martian mineralogy. *Journal of Geophysical Research*, 87(B12), 10115–10128. <https://doi.org/10.1029/jb087i12p10115>
- Moskowitz, B. M., & Hargraves, R. B. (1984). Magnetic cristobalite (?): A possible new magnetic phase produced by the thermal decomposition of nontronite. *Science*, 225(4667), 1152–1154. <https://doi.org/10.1126/science.225.4667.1152>
- Moskowitz, B. M., Jackson, M., & Kissel, C. (1998). Low-temperature magnetic behavior of titanomagnetites. *Earth and Planetary Science Letters*, 157(3–4), 141–149. [https://doi.org/10.1016/s0012-821x\(98\)00033-8](https://doi.org/10.1016/s0012-821x(98)00033-8)
- Nagata, T. (1961). *Rock magnetism*. Maruzen Company.
- Nagata, T., & Akimoto, S. (1956). Magnetic properties of ferromagnetic ilmenites. *Geofisica Pura e Applicata*, 34(1), 36–50. <https://doi.org/10.1007/bf02122815>
- Néel, L. (1955). Some theoretical aspects of rock-magnetism. *Advances in Physics*, 4(14), 191–243. <https://doi.org/10.1080/00018735500101204>
- Nilsson, A., Holme, R., Korte, M., Suttie, N., & Hill, M. (2014). Reconstructing Holocene geomagnetic field variation: New methods, models and implications. *Geophysical Journal International*, 198(1), 229–248. <https://doi.org/10.1093/gji/ggu120>
- Novikov, I. S., Sokol, E. V., Travin, A. V., & Novikova, S. A. (2008). Signature of Cenozoic orogenic movements in combustion metamorphic rocks: Mineralogy and geochronology (example of the Salair-Kuznetsk Basin transition). *Russian Geology and Geophysics*, 49(6), 378–396. <https://doi.org/10.1016/j.rgg.2007.11.011>
- Novikova, S., Sokol, E., & Khvorov, P. (2016). Multiple combustion metamorphic events in the Goose Lake Coal Basin, Transbaikalia, Russia: First dating results. *Quaternary Geochronology*, 36, 38–54. <https://doi.org/10.1016/j.quageo.2016.08.001>
- Ohkoshi, S., Namai, A., Imoto, K., Yoshikiyo, M., Tarora, W., Nakagawa, K., et al. (2015). Nanometer-size hard magnetic ferrite exhibiting high optical-transparency and nonlinear optical-magnetolectric effect. *Scientific Reports*, 5(1), 1–9. <https://doi.org/10.1038/srep14414>
- Özdemir, Ö., & Dunlop, D. J. (2000). Intermediate magnetite formation during dehydration of goethite. *Earth and Planetary Science Letters*, 177(1–2), 59–67. [https://doi.org/10.1016/s0012-821x\(00\)00032-7](https://doi.org/10.1016/s0012-821x(00)00032-7)
- Panovska, S., Constable, C. G., & Korte, M. (2018). Extending global continuous geomagnetic field reconstructions on timescales beyond human civilization. *Geochemistry, Geophysics, Geosystems*, 19(12), 4757–4772. <https://doi.org/10.1029/2018GC007966>
- Pavón-Carrasco, F. J., Osete, M. L., Torta, J. M., & De Santis, A. (2014). A geomagnetic field model for the Holocene based on archaeomagnetic and lava flow data. *Earth and Planetary Science Letters*, 388, 98–109. <https://doi.org/10.1016/j.epsl.2013.11.046>
- Petersen, N., Schembera, N., Schmidbauer, E., & Vali, H. (1987). Magnetization, Mössbauer spectroscopy and structural studies of a ferromagnetic Fe-oxide formed by heating nontronite in air. *Physics and Chemistry of Minerals*, 14(2), 118–121. <https://doi.org/10.1007/bf00308215>
- Rădan, S., & Rădan, M. (1998). Rock magnetism and paleomagnetism of porcelanites/clinkers from the western Dacic Basin (Romania). *Geologica Carpathica*, 49, 209–211.
- Reiners, P. W., Riihimäki, C. A., & Heffern, E. L. (2011). Clinker geochronology, the first glacial maximum, and landscape evolution in the northern Rockies. *Geological Society of America Today*, 21(7), 4–9. <https://doi.org/10.1130/G107A.1>
- Riihimäki, C. A., & Reiners, P. W. (2012). Empirical evidence of climate's role in Rocky Mountain landscape evolution. *Journal of Geophysical Research*, 117(2). <https://doi.org/10.1029/2011JF002137>

- Riihimaki, C. A., Reiners, P. W., & Heffern, E. L. (2009). Climate control on quaternary coal fires and landscape evolution, Powder River Basin, Wyoming and Montana. *Geology*, 37(3), 255–258. <https://doi.org/10.1130/G25195A.1>
- Roberts, S. B., Wilde, E. M., Rossi, G. S., Blake, D., Bader, L. R., Ellis, M. S., et al. (1999). *Colstrip Coalfield, Powder River Basin, Montana: Geology, coal quality, and coal resources*. US Geological Survey Professional Paper.
- Ron, H., & Kolodny, Y. (1992). Combustion Ayyalon area outcrop Anticline Normal fault. *Synclin*, 97, 6927–6939. <https://doi.org/10.1029/91jb03072>
- Sarnecki, J. C. (1991). Formation of clinker and its effects on locating and limiting coal resources. In *Geology in coal resource utilization*. Sokol, E. V., Novikova, S. A., Alekseev, D. V., & Travin, A. V. (2014). Natural coal fires in the Kuznetsk Coal basin: Geologic causes, climate, and age. *Russian Geology and Geophysics*, 55(9), 1043–1064. <https://doi.org/10.1016/j.rgg.2014.08.001>
- Sokol, E. V., & Volkova, N. I. (2007). Combustion metamorphic events resulting from natural coal fires. *GSA Reviews in Engineering Geology*, 18, 97–115. [https://doi.org/10.1130/2007.4118\(07\)](https://doi.org/10.1130/2007.4118(07))
- Sprain, C. J., Feinberg, J. M., Lamers, R., & Bono, R. K. (2021). 2021_Clinker. *Magnetic information consortium*. <https://doi.org/10.7288/V4/MAGIC/19216>
- Sprain, C. J., Feinberg, J. M., Renne, P. R., & Jackson, M. (2016). Importance of titanohematite in detrital remanent magnetizations of strata spanning the Cretaceous–Paleogene boundary, Hell Creek region, Montana. *Geochemistry, Geophysics, Geosystems*, 17(3), 660–678. <https://doi.org/10.1002/2015gc006191>
- Sternberg, R. S. (2009). Magnetic surveys and rock magnetic properties of clinkers in the Williston Basin. AGU Fall Meeting Abstracts (Vol. 2009, p. GP42A-01).
- Sternberg, R. S., Sparks, A., & Knudtson, O. (2008). *Magnetic surveys over burning and remediated coal seam fires in Western North Dakota*. Symposium on the application of geophysics to engineering and environmental problems 2008, Society of Exploration Geophysicists (pp. 389–398). <https://doi.org/10.4133/1.2963279>
- Stracher, G. B., Prakash, A., & Sokol, E. V. (2010). *Coal and peat fires: A global perspective: Volume 1: Coal-geology and combustion* (Vol. 1). Elsevier.
- Strauss, B. E., Strehlau, J. H., Lascu, I., Dorale, J. A., Penn, R. L., & Feinberg, J. M. (2013). The origin of magnetic remanence in stalagmites: Observations from electron microscopy and rock magnetism. *Geochemistry, Geophysics, Geosystems*, 14(12), 5006–5025. <https://doi.org/10.1002/2013gc004950>
- Tarduno, J. A., Cottrell, R. D., Watkeys, M. K., Hofmann, A., Doubrovine, P. V., Mamajek, E. E., et al. (2010). Geodynamo, solar wind, and magnetopause 3.4 to 3.45 billion years ago. *Science*, 327(5970), 1238–1240. <https://doi.org/10.1126/science.1183445>
- Tauxe, L., Bertram, H. N., & Seberino, C. (2002). Physical interpretation of hysteresis loops: Micromagnetic modeling of fine particle magnetite. *Geochemistry, Geophysics, Geosystems*, 3(10), 1–22. <https://doi.org/10.1029/2001gc000241>
- Tauxe, L., & Staudigel, H. (2004). Strength of the geomagnetic field in the Cretaceous Normal Superchron: New data from submarine basaltic glass of the Troodos Ophiolite. *Geochemistry, Geophysics, Geosystems*, 5. <https://doi.org/10.1029/2003GC000635>
- Thellier, E., & Thellier, O. (1959). Sur l'intensité du champ magnétique terrestre dans le passé historique et géologique. *Annales Geophysicae*, 15, 285–376.
- Tucek, J., Zboril, R., Namai, A., & Ohkoshi, S. (2010). $\epsilon\text{-Fe}_2\text{O}_3$: An advanced nanomaterial exhibiting giant coercive field, millimeter-wave ferromagnetic resonance, and magnetoelectric coupling. *Chemistry of Materials*, 22(24), 6483–6505.
- von Dobeneck, T. (1996). A systematic analysis of natural magnetic mineral assemblages based on modelling hysteresis loops with coercivity-related hyperbolic basis functions. *Geophysical Journal International*, 124(3), 675–694. <https://doi.org/10.1111/j.1365-246x.1996.tb05632.x>
- Wang, D., & Van der Voo, R. (2004). The hysteresis properties of multidomain magnetite and titanomagnetite/titanomaghemite in mid-ocean ridge basalts. *Earth and Planetary Science Letters*, 220(1–2), 175–184. [https://doi.org/10.1016/s0012-821x\(04\)00052-4](https://doi.org/10.1016/s0012-821x(04)00052-4)
- Wessling, S., Kuenzer, C., Kessels, W., & Wuttke, M. W. (2008). Numerical modeling for analyzing thermal surface anomalies induced by underground coal fires. *International Journal of Coal Geology*, 74(3–4), 175–184. <https://doi.org/10.1016/j.coal.2007.12.005>
- Whipkey, C. E., Cavaroc, V. V., & Flores, R. M. (1991). *Uplift of the Bighorn Mountains, Wyoming and Montana—A sandstone provenance study*. US Government Printing Office.
- Xu, H., Lee, S., & Xu, H. (2017). Luogufengite: A new nano-mineral of Fe_2O_3 polymorph with giant coercive field. *American Mineralogist*, 102(4), 711–719. <https://doi.org/10.2138/am-2017-5849>
- Yu, Y., Tauxe, L., & Genevey, A. (2004). Toward an optimal geomagnetic field intensity determination technique. *Geochemistry, Geophysics, Geosystems*, 5(2). <https://doi.org/10.1029/2003gc000630>
- Zhao, X., Roberts, A. P., Heslop, D., Paterson, G. A., Li, Y., & Li, J. (2017). Magnetic domain state diagnosis using hysteresis reversal curves. *Journal of Geophysical Research: Solid Earth*, 122(7), 4767–4789. <https://doi.org/10.1002/2016JB013683>

References From the Supporting Information

- Day, R., Fuller, M., & Schmidt, V. A. (1977). Hysteresis properties of titanomagnetites: Grain-size and compositional dependence. *Physics of the Earth and Planetary Interiors*, 13(4), 260–267. [https://doi.org/10.1016/0031-9201\(77\)90108-x](https://doi.org/10.1016/0031-9201(77)90108-x)
- Egli, R. (2013). VARIFORC: An optimized protocol for calculating non-regular first-order reversal curve (FORC) diagrams. *Global and Planetary Change*, 110, 302–320. <https://doi.org/10.1016/j.gloplacha.2013.08.003>
- Harrison, R. J., & Feinberg, J. M. (2008). FORCinel: An improved algorithm for calculating first-order reversal curve distributions using locally weighted regression smoothing. *Geochemistry, Geophysics, Geosystems*, 9(5). <https://doi.org/10.1029/2008gc001987>
- Néel, L. (1955). Some theoretical aspects of rock-magnetism. *Advances in Physics*, 4(14), 191–243. <https://doi.org/10.1080/00018735500101204>
- Tauxe, L., Bertram, H. N., & Seberino, C. (2002). Physical interpretation of hysteresis loops: Micromagnetic modeling of fine particle magnetite. *Geochemistry, Geophysics, Geosystems*, 3(10), 1–22. <https://doi.org/10.1029/2001gc000241>
- von Dobeneck, T. (1996). A systematic analysis of natural magnetic mineral assemblages based on modelling hysteresis loops with coercivity-related hyperbolic basis functions. *Geophysical Journal International*, 124(3), 675–694. <https://doi.org/10.1111/j.1365-246x.1996.tb05632.x>
- Wang, D., & Van der Voo, R. (2004). The hysteresis properties of multidomain magnetite and titanomagnetite/titanomaghemite in mid-ocean ridge basalts. *Earth and Planetary Science Letters*, 220(1–2), 175–184. [https://doi.org/10.1016/s0012-821x\(04\)00052-4](https://doi.org/10.1016/s0012-821x(04)00052-4)